A Case Study of Mid-Atlantic Nocturnal Boundary Layer Events during WAVES 2006

S. RABENHORST

Department of Physics, University of Maryland, Baltimore County, Baltimore, Maryland

D. N. WHITEMAN

Mesoscale Atmospheric Processes Laboratory, NASA Goddard Space Flight Center, Greenbelt, Maryland

D.-L. ZHANG

Department of Atmospheric and Oceanic Science, University of Maryland, College Park, College Park, Maryland

B. DEMOZ

Department of Physics and Astronomy, Howard University, Washington, D.C.

(Manuscript received 13 November 2013, in final form 11 June 2014)

ABSTRACT

The Water Vapor Variability-Satellite/Sondes (WAVES) 2006 field campaign provided a contiguous 5-day period of concentrated high-resolution measurements to examine finescale boundary layer phenomena under the influence of a summertime subtropical high over the mid-Atlantic region that is characterized by complex geography. A holistic analytical approach to low-level wind observations was adopted to identify the low-level flow structures and patterns of evolution on the basis of airmass properties and origination. An analysis of the measurements and the other available observations is consistent with the classic depiction of the daytime boundary layer development but revealed a pronounced diurnal cycle that was categorized into three stages: (i) daytime growth of the convective boundary layer, (ii) flow intensification into a low-level jet regime after dusk, and (iii) interruption by a downslope wind regime after midnight. The use of the field campaign data allows for the differentiation of the latter two flow regimes by their directions with respect to the orientation of the Appalachian Mountains and their airmass origins. Previous studies that have investigated mountain flows and low-level jet circulations have focused on regions with overt geographic prominence, stark gradients, or frequent reoccurrences, whereby such meteorological phenomena exhibit a clear signature and can be easily isolated and diagnosed. The results of this study provide evidence that similar circulation patterns operate in nonclassic locations with milder topography and atmospheric gradients, such as the mid-Atlantic region. The new results have important implications for the understanding of the mountain-forced flows and some air quality problems during the nocturnal period.

1. Introduction

The nocturnal low-level jet (LLJ) is a locally generated atmospheric flow pattern that frequently impacts the mid-Atlantic region during the warm season (Zhang et al. 2006). It is believed to be a significant mechanism for the regional transport and redistribution of pollutants (Delgado et al. 2014; Weldegaber et al. 2013, manuscript submitted to *Meteor. Atmos. Phys.*), often creating a favorable environment (Ryan et al. 1998) that can enhance or reduce air quality during subsequent days. To this day, there have been relatively few publications on U.S. east coast LLJs as compared with those examining the well-studied Great Plains LLJ (Bonner 1968; Jiang et al. 2007; Parish et al. 1988; Song et al. 2005). Nevertheless, there is a growing awareness that these features occur around the world with varying characteristics (Rife et al. 2010). While more research is needed in understudied areas, such as the East Coast, there has been some notable literature documenting

Corresponding author address: S. Rabenhorst, Dept. of Physics, University of Maryland, Baltimore County, Baltimore, MD 21250. E-mail: sraben1@umbc.edu

DOI: 10.1175/JAMC-D-13-0350.1

LLJ occurrences in Florida (Karipot et al. 2009), the Carolinas (Sjostedt et al. 1990), the mid-Atlantic (Zhang et al. 2006), Pennsylvania (Verghese et al. 2003), and New York (Colle and Novak 2010). To better understand the development of East Coast LLJs, more attention should be given to understanding the local mechanisms driving them.

Previous studies have used various criteria to define LLJ events, such as fixed (Banta et al. 2002; Whiteman et al. 1997) and relative (Andreas et al. 2000; Zhang et al. 2006) maximum wind speeds and falloffs (Bonner 1968; Sjostedt et al. 1990), or a combination of the above (Baas et al. 2009). While most literature uses the wind speed profile as the principal metric for LLJ determination, this approach may inadvertently include other low-level wind regimes driven by completely different mechanisms than those associated with the classic notion of LLJs, as in the Great Plains (Parish et al. 1988; Song et al. 2005; Whiteman et al. 1997). Since the term LLJ is literally true for other low-level wind phenomena, such as winds associated with cyclones or frontal passages, we draw a distinction in this paper and, hereafter, refer to an LLJ as a subset of wind speed maxima describing nocturnal low-level wind flow moving parallel to local topographical gradients in the absence of synoptic-scale forcing mechanisms. In the mid-Atlantic region, this motion is oriented, more or less, parallel to the Appalachian Mountains, resulting in a south-southwesterly wind. These types of LLJs are characterized by the development of a layer of fast-moving air, which can become supergeostrophic, following the inertial oscillation of the atmosphere brought about by a sudden frictional decoupling near sunset (Blackadar 1957; Holton 1967) and thermal gradients over sloping terrain (Parish and Oolman 2010).

Another type of low-level mesoscale flow is downslope winds (DWs), generated by cross-barrier terrain-induced gravity waves (Durran 2003; Klemp and Lilly 1975). DW events associated with mountain wave amplification and breaking waves have been well documented in large mountain ranges around the world (Colman and Dierking 1992; Grisogono and Belušić 2009; Klemp and Lilly 1975; Koletsis et al. 2009; Nkemdirim 1986; Raphael 2003; Seluchi et al. 2003). Previous research on DWs has gravitated toward cases and regions where damaging windstorms occur (Blier 1998; Brinkmann 1974; Meyers et al. 2003). Such events usually occur in areas with steep terrain or high-mountain profiles. However, mountains with lower elevations and more gentle slopes, such as the Appalachians, have also demonstrated the capability of producing DWs (Decker and Robinson 2011; Gaffin 2009). In fact, DWs do not have to be severe or damaging to be present and are frequently found in mountain lee areas. The case study in this paper presents DW events from a different perspective, where the focus is not on high speed winds but rather the downstream effects of reoccurring, mild DWs over the central Appalachian Mountains. These flows have the ability to impact mid-Atlantic air quality and locally modify existing wind circulations. A distinct characteristic of DW events as compared with LLJ events is that the wind flow is oriented perpendicular to mountain ridges, which is in agreement with the findings of Colle and Mass (1998). DWs may be lofted depending on the observing location with respect to their length scale. The length and intensity of DWs are governed by many factors, such as the inversion height and surface heat fluxes (Smith and Skyllingstad 2011). Several studies have shown that DWs preferentially occur during the late afternoon or nighttime hours (Brinkmann 1974; Grubisic and Xiao 2006; Seluchi et al. 2003), which may be facilitated by a negative surface heat flux (Smith and Skyllingstad 2009).

While previous studies have separately examined LLJ and DW events, the aim of this study is to show the cyclical, dynamic interplay of these two features and how they affected the planetary boundary layer (PBL) during a 5-day period in 2006 over the Baltimore, Maryland–Washington, D.C., region with complex geography. The objectives of this paper are to (i) combine several research measurements into analytical tools that can be used to detect and discern the evolution of low-level flows, (ii) demonstrate the presence of two distinct nocturnal low-level flows that could be misconstrued as a single LLJ event, and (iii) explore the respective roles of these two distinct flows in significantly modifying the lowest 1–2-km profile of the atmospheric flows. The next section provides a brief overview of the Water Vapor Variability-Satellite/Sondes (WAVES) 2006 field campaign and instrumentation. Section 3 describes the synoptic setting and meteorology during the case study. Section 4 presents the observation data, followed by a discussion and conclusions in the final section.

2. Data sources and WAVES

The WAVES field campaign commenced 27 June 2006 and continued until 12 August 2006. Measurements were centered at the Howard University Beltsville Research Campus (HUBRC) in Beltsville, Maryland, located between Baltimore and Washington at 39.05°N, 76.88°W with an elevation of 52 m above sea level (Fig. 1). The campaign was a collaborative effort among several government agencies and universities including the National Aeronautics and Space Administration Goddard Space Flight

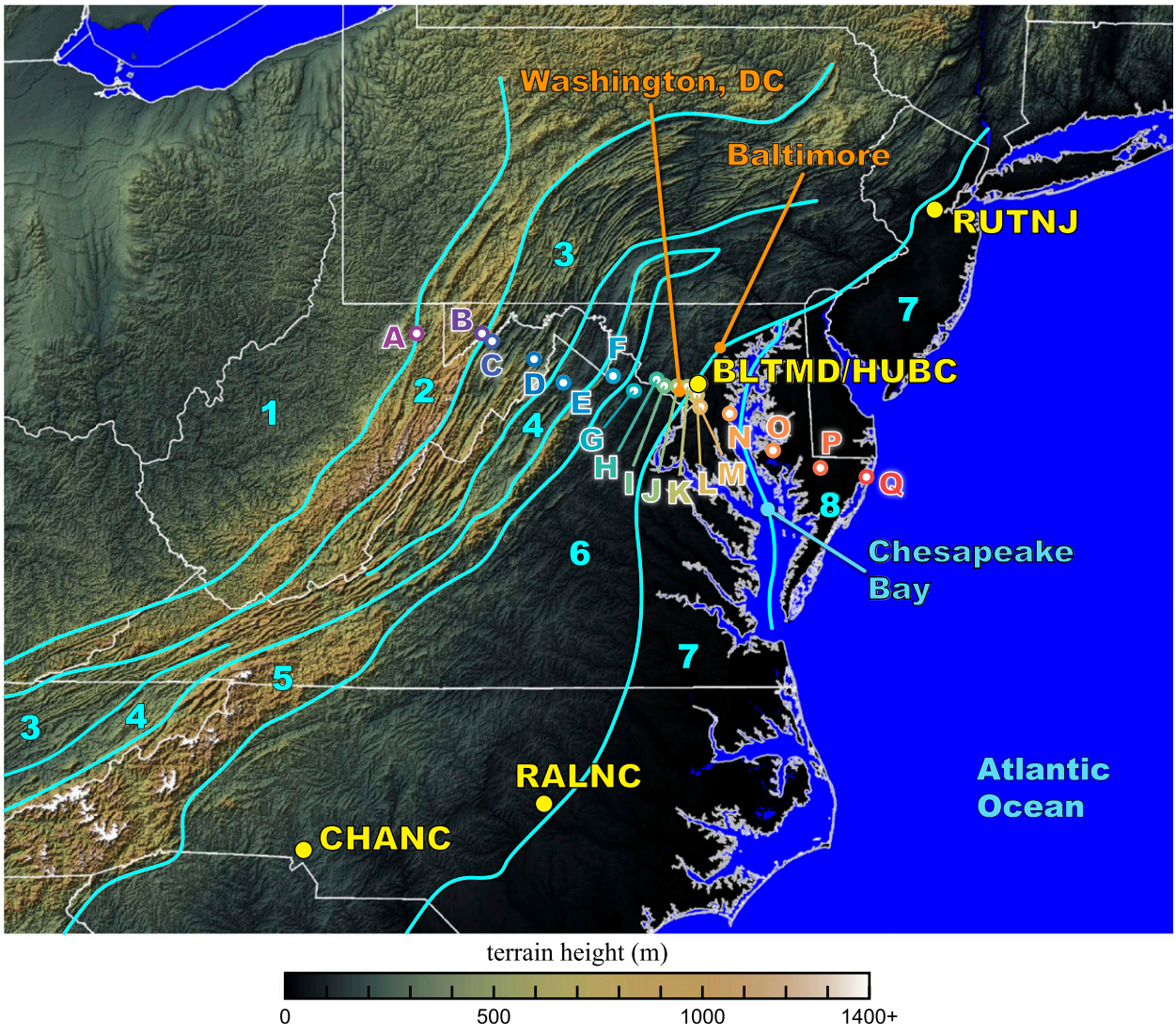

FIG. 1. The mid-Atlantic region with seven distinct geographies separated by cyan lines: the 1) Western Upslope, 2) Appalachian Mountain Highlands, 3) Ridge and Valley, 4) Great Valley, 5) Blue Ridge Mountains, 6) Piedmont Plateau, and 7) Coastal Plains regions. The Coastal Plains are further subdivided into the 7) Western and 8) Eastern Shores to the west and east of the Chesapeake Bay, respectively. Locations A–Q are WeatherBug sites selected to observe surface winds. The nearest operational wind profilers during this case study are labeled in yellow. The distances between the profiler sites and the Appalachian Mountains were approximately 30, 75, 125, and 190 km for RUTNJ, BLTMD, CHANC, and RALNC, respectively.

Center (NASA GSFC); the National Oceanic and Atmospheric Administration/National Weather Service; Howard University; the University of Maryland, Baltimore County; The Pennsylvania State University; the University of Maryland, College Park; and Maryland's Department of the Environment (MDE). The primary objective of the WAVES 2006 field campaign was to acquire a robust set of coordinated measurements that could be used for satellite validation and inter-instrument comparison, assessing satellite variability and accuracy, with an emphasis on water vapor, ozone, temperature, and aerosol profiles.

Another aim of WAVES 2006 was to analyze case studies of regional-scale meteorological events. Therefore, an intensive phase of the field campaign began in early August in anticipation of a series of days with poor air quality that would culminate with the passage of a weak summertime cold front. Round-the-clock measurements were conducted with the goal of capturing the pre- and postfrontal meteorology. This generated a continuous dataset of finescale observations that showed the passage of a prefrontal trough and a cold front, and revealed a detailed view of the diurnal evolution of the PBL. This paper documents this case study of 1–5 August 2006.

A host of ground-based and in situ sensors contributed to WAVES field operations, including nine lidar systems, 10 different radiosonde technologies, Doppler C-band radar, a wind profiler and radio acoustic sounding system (RASS), a microwave radiometer, a ceilometer, a whole-sky imager, broadband and spectral radiometers, Suominet GPS total column measurements, and several air quality instruments measuring trace gases and particulates. In addition, a 31-m instrumented tower extended just above the tree canopy. Wind, temperature, humidity, and radiation sensors were located at various heights on the tower to allow surface flux measurements. All of the measurements discussed in this paper were acquired within a few hundred meters of each other on the HUBRC site unless otherwise noted.

Research lidar systems were among the most useful instruments of the WAVES campaign because they provided a detailed evolution of the lower atmosphere through continuous high-resolution measurements. The lidar data presented in this paper were acquired by the NASA GSFC scanning Raman lidar (SRL; Whiteman et al. 2004, 2006), with the exception of a small time gap from 0730 to 1045 UTC (LST = UTC − 4) 4 August when SRL was offline. Data were ''patched in'' from the Howard University Raman lidar, described in Adam et al. (2010). Both Raman lidar systems used a tripled Nd:YAG laser emitting in the near UV at 354.7 nm. This excitation wavelength produces Raman-shifted scattering for nitrogen, and water vapor centered near 386.7 and 407.5 nm, respectively. The water vapor mixing ratio (WVMR) is derived by comparing the water vapor signal with that of nitrogen, which composes a near-uniform 78% of the lower atmosphere (Goldsmith et al. 1998; Melfi et al. 1989; Turner et al. 2000; Whiteman et al. 1992; Whiteman 2003). The aerosol scattering ratio (ASR) was another product that was helpful in diagnosing different air masses. ASR is derived from the ratio of Mie scattering (including nonspherical objects) to molecular scattering (Ferrare et al. 2006; Whiteman 2003). ASR data typically have high values for strong scatterers, such as particulate matter, pollutants, dust, pollen, or cloud droplets. The WVMR and ASR data in this paper were collected using a zenith-orientated beam with vertical and temporal resolutions of 30 m and 1 min, respectively.

Another important instrument during the WAVES campaign was the MDE 915-MHz radar wind profiler with RASS. Depending on the atmospheric conditions, this system provided continuous PBL wind data from near the surface up to a maximum of 4 km. However, a decreasing signal to noise ratio above 3 km above ground level (AGL) generally restricted the valid data to lower levels. The temporal and vertical resolutions of the wind data were 15 min and 90 m, respectively. More information about WAVES 2006, particularly the lidar measurements during the campaign, can be found in Adam et al. (2010).

3. Synoptic background

During the first week of August 2006, a surface frontal boundary progressed from the upper Great Plains down through the Carolinas. The major upper-level features controlling the eastern U.S. weather pattern were cyclonic centers tracking across Canada, and a quasi-stationary ridge that was located over the southeastern United States. The eastward progression and timing of the surface cold front were governed by the interplay of these large-scale features. Figure 2a shows the 500-hPa heights and the position of the surface cold front at 0000 UTC 3 August, before the front passed through the mid-Atlantic. Over the period of 3–4 August, the cyclonic region L2 merged with L1, forming an elongated short-wave trough (axis oriented southward) that facilitated the repositioning of the blocking anticyclonic centers H1 and H2. This sequence of events allowed the surface cold front to finally move through the mid-Atlantic region, after virtually stalling in the Midwest region from 1 to 3 August. By 0000 UTC 6 August (Fig. 2b), the cold front completely cleared the mid-Atlantic region. Although the frontal boundary was marked by a line of precipitation in the Midwest, the convective activity diminished and became less organized as the front approached the Appalachian Mountains. There was virtually no precipitation associated with the front east of the Appalachian Mountains within the mid-Atlantic region. Therefore, the frontal passage through this region was considered a ''weak'' cold front because the atmospheric gradients across the boundary were more subtle, and it generated shallow convection and minimal rainfall. The two most notable meteorological events observed at HUBRC during this case study were the passages of a prefrontal trough around 2100 UTC 3 August (Fig. 2c) and the surface cold front between 2100 and 2300 UTC 4 August (Fig. 2d). The prefrontal trough propagated ahead of the cold front, exhibiting a minimum in surface pressure, a wind shift, and other characteristics that were similar to the discussion of prefrontal troughs by (Schultz 2005). The cold front made a dry passage through the HUBRC site, bringing slightly cooler and much drier postfrontal air to the region. Figure 2d illustrates how the surface roughness of the Appalachian Mountains provided sufficient drag to distort the cold-frontal boundary as it crossed the mountain barrier. The postfrontal air from Pennsylvania–New Jersey arrived at HUBRC first,

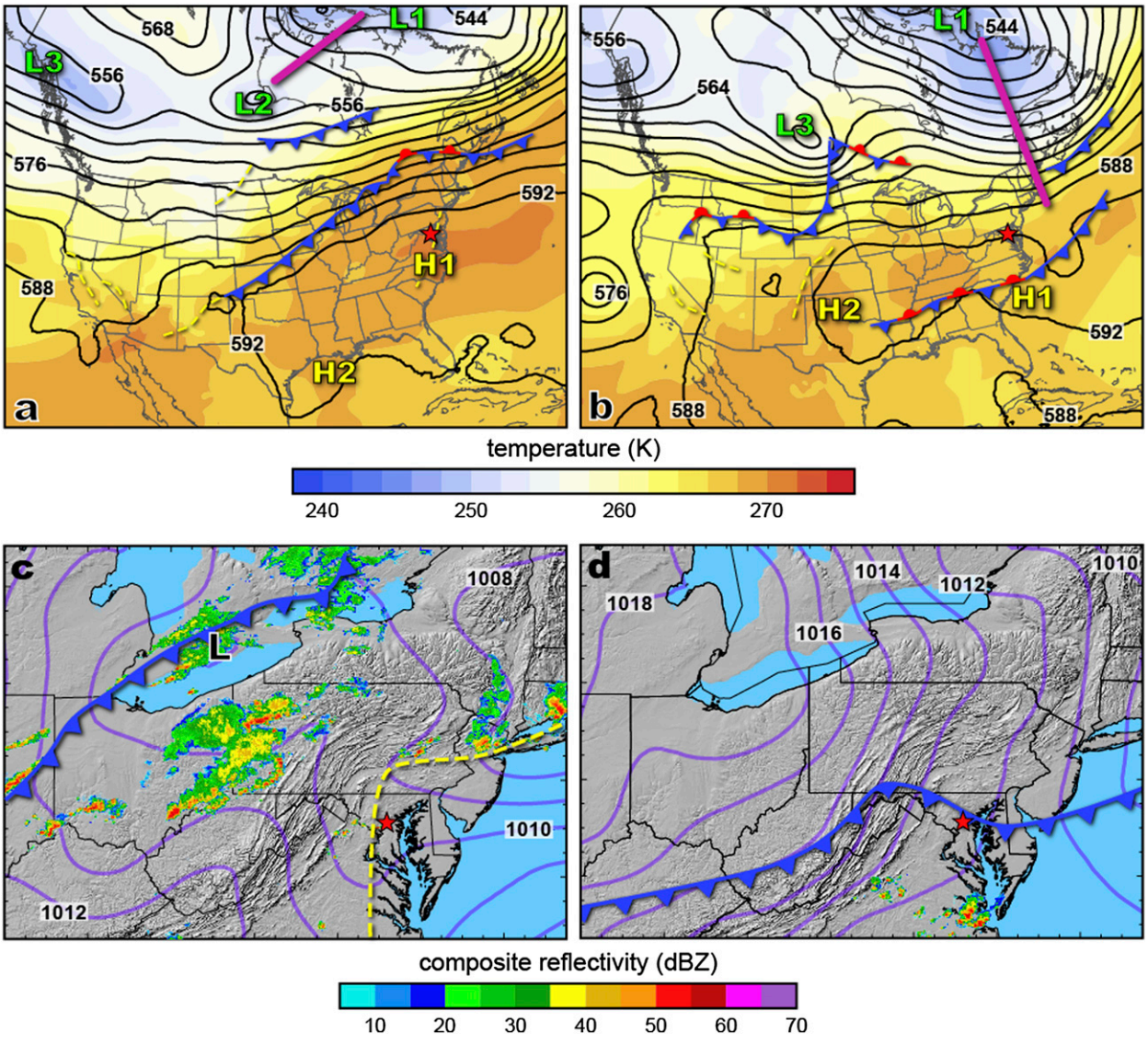

FIG. 2. (top) NARR reanalysis of 500-hPa temperature (shading) and geopotential height (contours), superimposed with frontal boundaries and troughs (short yellow dashed lines) from Unisys surface analysis. The purple line identifies a short-wave trough rotating around L1. Reanalysis times are at (a) 0000 UTC 3 Aug and (b) 0000 UTC 6 Aug 2006. (bottom) Next Generation Weather Radar (NEXRAD) composite radar reflectivity (dBZ) and RUC sea level pressure contours (hPa) overlaid on the topographical shaded relief at (c) 2300 UTC 3 Aug and (d) 2100 UTC 4 Aug. The surface cold front (blue line) and prefrontal trough (yellow dashed lines) are drawn based on the 950-hPa RUC analysis temperature and sea level pressure fields. HUBRC is identified by the red star.

because traversing the lower terrain to the north provided less resistance to the advancing air mass than did the more rugged Virginia–West Virginian mountains west of HUBRC. Therefore, the boundary effectively folded over the HUBRC site, with a second flow reinforcing of postfrontal air from the west after the boundary cleared the higher terrains in VA–WV.

Both the prefrontal trough and cold-frontal events marked a transition between air masses. The dominant daytime wind direction in the PBL transitioned from westerly to northwesterly after the passage of the prefrontal trough, then from northwesterly to north-northeasterly after the cold front. Each transition was marked by a reduction in humidity.

4. Analysis of diurnal variations

a. WAVES profiling

A continuous PBL profile time series of lidar and wind profiler measurements from 1 to 5 August is presented in Fig. 3, showing a pronounced diurnal cycle of the low-level

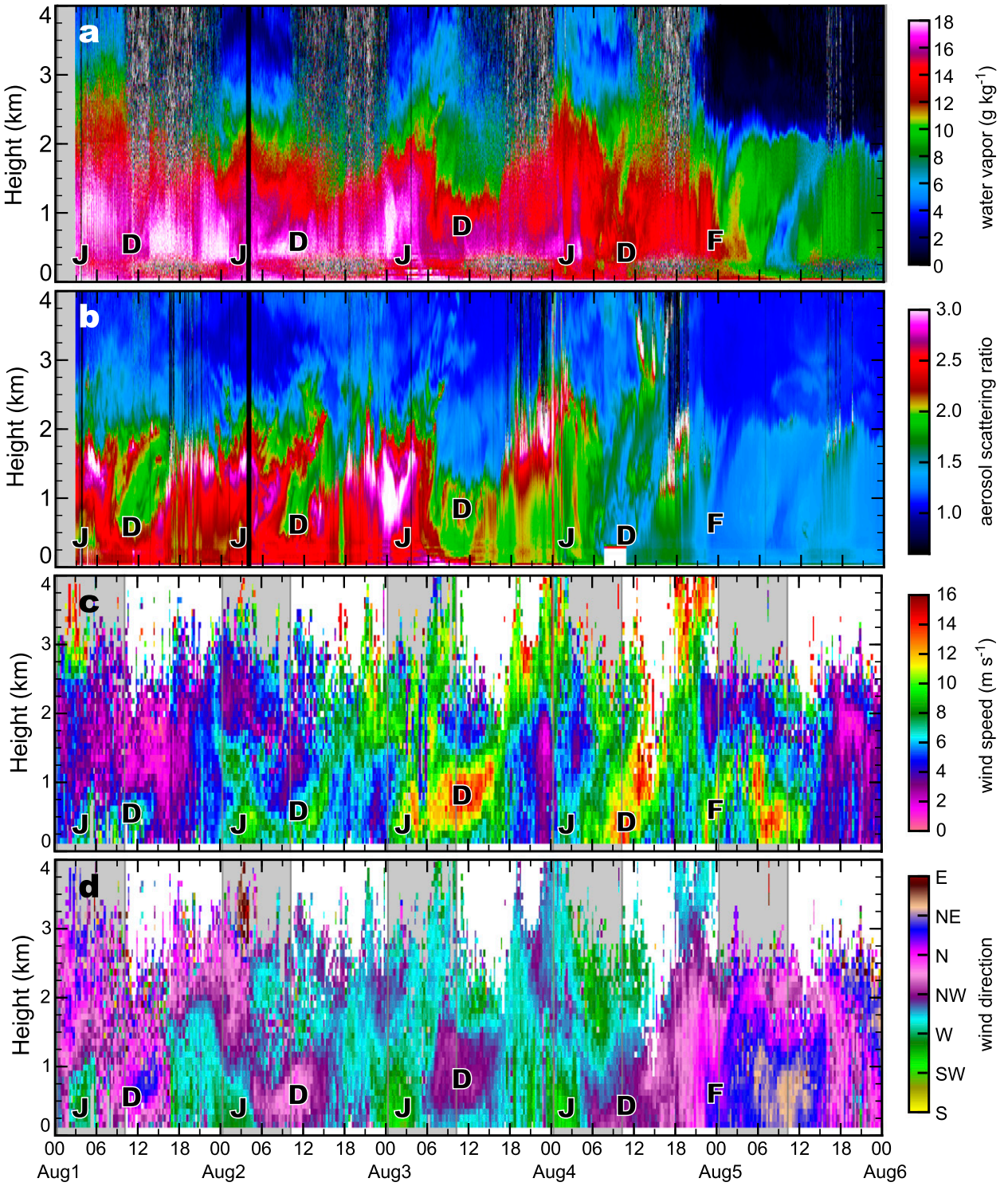

FIG. 3. HUBRC 4 km AGL time series from 0000 UTC 1 Aug to 0000 UTC 6 Aug 2006. Shown are (a) SRL water vapor mixing ratio, (b) SRL aerosol scattering ratio, and MDE wind profiler (c) speed and (d) direction. Gray-shaded background indicates nighttime periods. Letters J, D, and F designate the LLJ, downslope winds, and cold-frontal events, respectively; as in the rest of figures.

meteorology at HUBRC during this case study. Three distinct features are apparent: an LLJ regime (denoted by a J), a DW regime (denoted by a D), and the passage of the surface cold front (denoted by an F), which was followed by a large decrease in WVMR (Fig. 3a) and ASR (Fig. 3b). The DW and LLJ regimes can be identified by their unique characteristics. The DW flow corresponded to a significant reduction in the ASR (Fig. 3b), and a slight reduction in WVMR (Fig. 3a), between 0.8 and 2.5 km AGL and 0600 and 1500 UTC. During this period, the DW winds below 1.5 km AGL were northwesterly (purple shading in Fig. 3d) with a peak value located between 200 and 1000 m (Fig. 3c). By comparison, the LLJ regime can be identified by a wind speed maximum in the lowest kilometer of the atmosphere with a west-southwesterly direction, which was perpendicular to the DW wind direction. The ASR values decreased slightly during the LLJ regime, perhaps most notably during the nights of 1–2 August. There was also a minor increase in WVMR associated with the LLJ regime.

The period of 1–4 August showed a diurnal signature due to the different regimes described above that became progressively more apparent with time. This was particularly evident in the nocturnal low-level wind speed field, which consistently increased with each subsequent day. This is consistent with the general expectation of stronger southwesterly flow ahead of the approaching cold front and nearby jet stream. Meanwhile, an anticyclonic region [500-hPa data from the North American Regional Reanalysis (NARR)] moved from Kentucky to the east of North Carolina, which allowed geostrophic winds above the PBL to gradually turn from the northwest to the west-southwest over the Beltsville site. It is conjectured that the increasingly southwesterly wind component might have facilitated LLJ development, while the increasing cross-barrier flow may have enhanced the DW intensity, contributing to a more pronounced diurnal cycle leading up to 5 August. For example, the dominant wind direction throughout 1 August was north-northwesterly (purple shading in Fig. 2d) except for a short interlude during the LLJ regime from 0200 to 0600 UTC. However, as time progressed, a layer of west-southwesterly flow (green-cyan hues in Fig. 2d) developed that was increasing in vertical extent and with time each day ahead of the cold front, and only interrupted by the daily DW events.

A careful examination of these finescale observations indicates that more complicated dynamics were at play than can be explained by synoptic-scale flows. The shallow layer of west-southwesterly flow remained confined to the lowest few kilometers of the atmosphere, but appeared to undergo a periodic lifting and descent each day. Undoubtedly, the CBL cycle was the primary driver of this pattern of lifting and descent. However, the airmass intrusions associated with the LLJ and DW regimes also contributed to subtle lifting within the lower atmosphere, with the latter being more pronounced. The overall effect of these events was to gradually lift the layer of west-southwesterly flow throughout the nighttime period, especially after the arrival of the DW regime. It should be emphasized that any vertical motion mentioned with respect to the passage of the LLJ or DW regimes was always an order of magnitude less than that associated with horizontal advection, which was clearly dominant and evidenced by the higher horizontal wind speeds in the cores of these features. During the afternoon periods (1600–2000 UTC) of 1–3 August, the layer of west-southwesterly flow reached its maximum thickness when the convective boundary layer (CBL) winds below ~1.5 km transitioned from north-northwesterly to west-southwesterly and became synchronized with wind direction in the lofted layer. During the early evening periods (2000–0000 UTC), the CBL height and buoyant processes began to diminish. In the absence of temperature profile measurements, a vertical gradient in wind direction was assumed to be a proxy for the location of the PBL height, with pseudo-isentropic motion above the PBL. During this time, the decaying PBL was evidenced by the decreasing thickness of the layer of southwesterly flow below the PBL top, and the appearance of northwesterly flow above 1.0, 1.5, and 2.0 km on 1, 2, and 3 August, respectively. A more lengthy discussion on these dynamics and the diurnal cycle will be presented in section 5.

b. *WAVES surface observations*

Several surface observations were acquired at the HUBRC site for the 5-day period (Fig. 4). Ground and tower observations were collected near the wind profiler and lidar systems. These observations also exhibited day-to-day patterns, indicative of the diurnal cycle described above.

Temperatures in the lowest 31 m exhibited small temperature deviations throughout the height of the tower during the daytime CBL and a more stratified environment with temperature differences of up to 5°C across the tower depth at night (Fig. 4a). Mixing-ratio data (Fig. 4c) acquired at the top and bottom of the tower showed similar variations of features although the values at the ground were approximately $2\,g\,kg^{-1}$ higher on average. The WVMR varied between approximately 18 and $20\,g\,kg^{-1}$, for the tower top and base, respectively, until 4 August. After that date, it steadily decreased to 9 and $11\,g\,kg^{-1}$, respectively, by 2100 UTC 5 August. It was of interest that the passage of the prefrontal trough marked the beginning of the humidity decrease rather than the cold front itself.

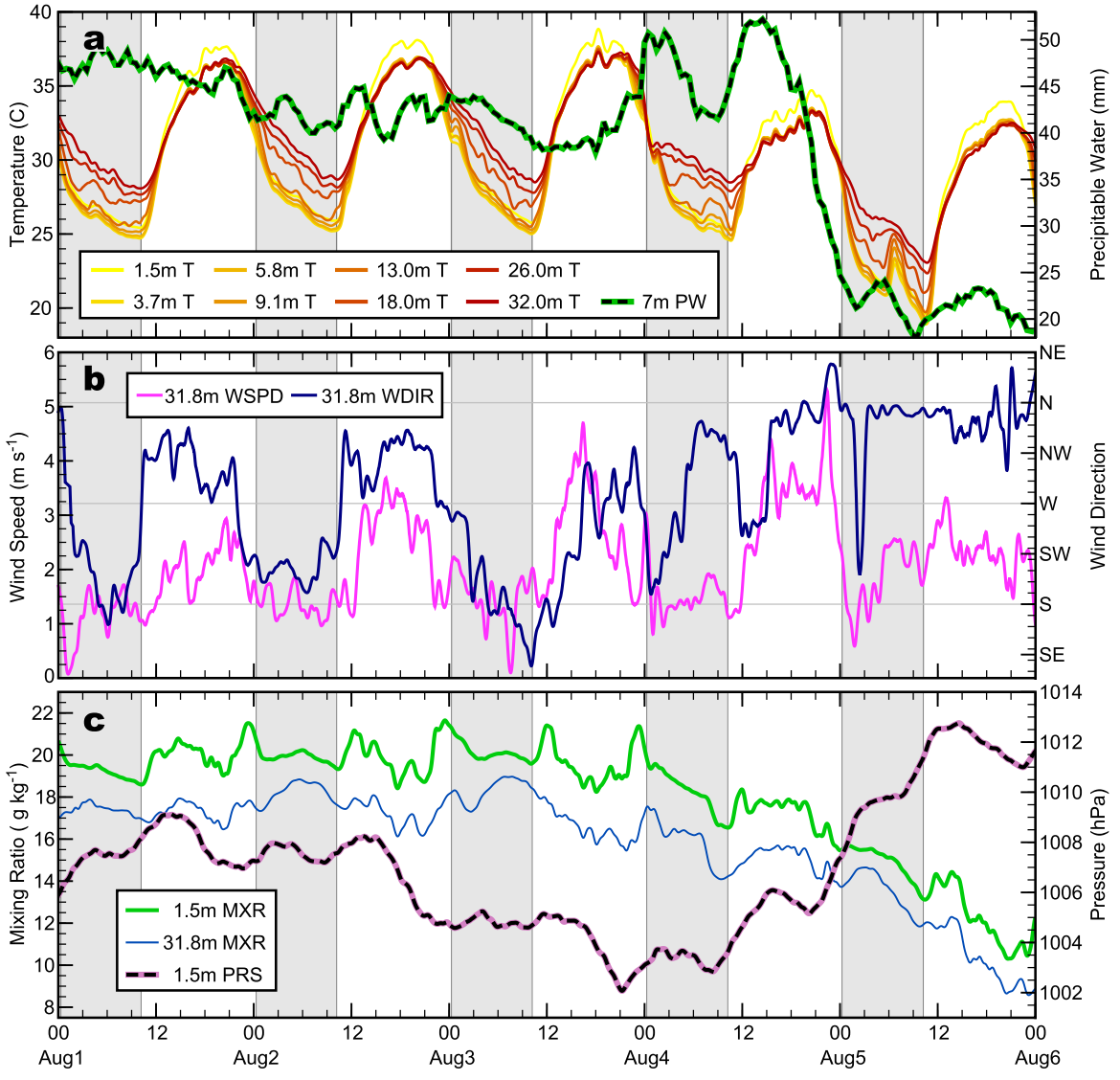

FIG. 4. Surface observations collected at HUBRC from 0000 UTC 1 Aug to 0000 UTC 6 Aug 2006: (a) precipitable water vapor and temperature from the 31-m meteorological tower, (b) wind speed and direction at the tower top, and (c) surface pressure and mixing ratio at the tower base and top. Gray-shaded background indicates nighttime periods.

There were a few notable features that were similar from day to day. During the 2–3 h prior to sunset, the water vapor at the surface spiked by ~2 g kg^{-1}. Since the HUBRC site was surrounded by a wooded area with swampy locations, it is speculated that the absence of convection during these times reduced the downward mixing of drier air, and calmer winds (Fig. 4b) did not efficiently ventilate a buildup of near-surface moisture. This would also explain why the 1.5-m spikes were more prominent compared to those at 31.8 m located slightly above the top of the tree canopy. For the remainder of the nighttime period, the mixing ratio values produced a convex curve in Fig. 4c, whereby the peak values coincided with the transition from the LLJ to the DW regime. The mixing ratio generally decreased after the arrival of the DW regime. While it is true that plant stomata are usually closed during the nighttime periods (Jones 1983), effectively shutting off transpiration, the convex signature was more prominent in the 31.8-m observations. This seems to indicate that the change was forced from above by ventilation processes. Shortly after sunrise, the 1.5-m mixing ratio values spiked again. The increase and decrease appear to be associated with a sudden change in wind direction and a sudden increase in wind speed, respectively. It is still unclear why these signatures are present in the

dataset, and more investigation is needed to determine their cause.

High-resolution surface wind data (Fig. 4b) were sampled at the top of the tower using sonic anemometers to explore the relationship with the wind profiler measurements that were available at altitudes of 250–750 m AGL, above the tower height of 31 m. At the surface, wind speeds were strongest during daytime hours with increasing magnitude each day ahead of the cold front, eventually exceeding 5 m s^{-1} on the afternoon of 4 August. Nocturnal winds were calmer with values around 1.5 m s^{-1}. Generally speaking, the strongest (weakest) wind speeds coincided with the warmest (coolest) surface temperature, which is a result similar to the findings of Zhang and Zheng (2004). These surface wind speeds were inversely related to those at higher elevations in the PBL, which clearly showed a pattern of stronger winds during the nighttime. In fact, from surface data alone (even at 31.8 m AGL, which was slightly above the tree canopy), one could see little indication of the ongoing LLJ and DW events that occurred higher above the surface.

The wind direction pattern at the surface was also different from that measured between 250 and 750 m AGL. There appeared to be a 3–4-h lag in the surface wind direction compared to that between 250 and 750 m AGL. The daytime surface wind direction was primarily northwesterly during 1–3 August, although the wind direction transition to northwesterly occurred more slowly on 3 August. By comparison, the wind direction between 250 and 750 m transitioned to northwesterly much earlier at night with the advent of the DW events. At the surface, this transition occurred much closer to dawn. During the nights of 1–3 August, the surface wind direction was mostly south-southwest and even rotated slightly southeasterly on the night of 3 August. After the passage of the prefrontal trough, the nocturnal wind direction on the morning of 4 August was only southwesterly for a brief time during the LLJ regime, and then it tended toward a direction that was mostly northwesterly. By comparison, the wind direction between 250 and 750 m transitioned to southwesterly much earlier in the afternoon. After the passage of the cold front, the surface wind lost its diurnal signature and became consistent northerly at ~2.5 m s^{-1} during both daytime and nighttime periods.

It is interesting to note the dramatic wind shifts that occurred near dawn in the prefrontal air mass. These signatures were not present in the wind profiler data at 250–750 m AGL. On 1–2 August, the wind abruptly changed from southwesterly to northwesterly at first daylight. On 3 August the transition was more gradual, but dawn clearly marked the time when the trend in wind direction was reversed. After the passage of the prefrontal trough, the wind direction broke the previous day's pattern and changed from northwesterly to southwesterly, but the timing was still contemporaneous with dawn. Wind speeds typically increased after a directional shift.

To explain the abrupt wind shifts measured in the layer near the surface compared to the winds measured between 250 and 750 m AGL, it is hypothesized that momentum synchronization may have occurred near dawn between the two layers, respectively. It is likely that atmospheric stability created a layered environment throughout the nighttime, particularly at low levels, which mitigated the depth and penetration of any shear-driven turbulent eddies, thereby insulating the lowest layers from any significant downward transport of horizontal momentum. After daybreak, surface heating could quickly dissolve the calmer shallow nocturnal surface layer and, thereby, allow convective eddies to transfer momentum downward causing an abrupt change in wind speed or direction. This concept can also explain the time lag in the change in near-surface wind direction compared to the winds at 250–750 m AGL. Unfortunately, there is a vertical gap in wind observations between the top of the 31 m tower and the lowest level of the wind profiler near 175 m. Radiosondes launched (0655 UTC 1 August and 0644 UTC 3 August) from HUBRC indicated the depth of the nocturnal surface layer was ~100 m. Therefore, the evolution and breakdown of this shallow surface layer after dawn would not have been captured by WAVES instrumentation. Interestingly, a reverse wind shift pattern occurred over a 3-h period just prior to sunset on 1–3 August. In those cases, the wind speeds rapidly decreased and then transitioned from northwesterly to southwesterly. Similarly, this appears indicative of a decoupling and momentum isolation of the lower atmosphere at the beginning of the nighttime. This theory offers some explanation as to why the DW and LLJ events were nondetectable in the surface data. More detailed studies that capture these levels of the atmosphere are needed to determine the exact evolution and mechanisms responsible for this surface wind behavior.

Figure 4c shows that the overall pressure trend was negative, reaching a 5-day minimum of 1002 hPa at 2100 UTC 3 August, which coincided with the passage of the prefrontal trough. Thereafter, it increased slightly to 1006 hPa by the time of the frontal passage. Afterward, the surface pressure rose rapidly to over 1012 hPa by 1200 UTC 5 August. Overriding the pressure tendency was the signature of the semidiurnal tide (Whiteman and Bian 1996). Every night there was a local maximum pressure around 0400 UTC and a minimum pressure

near 0700 UTC. Similarly, the local daytime maximum and minimum occurred near 1600 and 2100 UTC, respectively.

Total column precipitable water (PW) decreased slightly over the period of 1–3 August, ranging from 45 to 40 mm (Fig. 4a). The period of 0000–0300 UTC 3 August was characterized by a push of moisture immediately ahead of the cold front. This PW increase was associated with the northward transport of post-convective moisture from the Carolinas and southwestern Virginia through upper-level winds and the LLJ. A second PW maximum occurred around 1200–1600 UTC 4 August and was associated with moisture convergence immediately ahead of the frontal boundary. Throughout the evening of 4 August and into the nocturnal hours of 5 August, the PW decreased sharply by more than 30 mm due to the passage of the frontal boundary.

c. *Regional wind profilers*

The nearest operational wind profilers along the East Coast (Fig. 1) were examined to determine whether nocturnal phenomena similar to those uncovered in the WAVES observations were occurring at other locations, regionally. The Rutgers (RUTNJ, New Brunswick, New Jersey), Raleigh (RALNC, Raleigh, North Carolina), and HUBRC/Beltsville (BLTMD, Beltsville) wind profilers were all located along the Fall Line, which is a topographic transition between the rolling hills of the Piedmont (region 6 in Fig. 1) and the flat coastal plains to the east (region 7 in Fig. 1). The Fall Line is a geographic feature because it often channels or limits the westward extent of LLJs even though the elevation drop is small. The Charlotte site (CHANC, Charlotte, North Carolina) was located to the west of the Fall Line, well into the hillier Piedmont region.

Figures 5 and 6 compare the wind direction and speed between the four wind profiler sites. The LLJ and DW features were most clearly defined at BLTMD but distinguishable at all sites. The BLTMD wind profiler also had a finer resolution than the other three profilers. Overall, the nocturnal features at BLTMD had a shallower vertical extent (<1.5 km) than at the other sites. Wind speeds were typically greater at sites located farther north and closer to the vicinity of the frontal boundary, whereas calmer conditions presided farther south under the anticyclonic region H1 (Fig. 2).

The timing of the DW events at RUTNJ was similar to those at BLTMD but was elevated much higher at 500 m AGL. The DW events arrived later at the CHANC and RALNC sites. The 3–4-h lag is believed to be related to the increased distance from the Appalachian Mountains, assuming DW propagation speeds were similar. However, it is impossible to determine the exact propagation speeds from this dataset alone. DW events were less defined in the North Carolina sites, which could have been the result of spreading over a greater distance from the mountains. These southern events were more disorganized and had a frontlike appearance, showing a slight vertical slant over a much deeper layer. Here, the arrival of the DW regime was marked by a zone of increased wind speeds (4–6 m s^{-1}) from the surface slanted up to 3 km AGL. These DW wind speeds were very weak, and virtually indistinguishable from the background flow. In contrast, the DW events in the northern sites appeared more borelike with a core of higher wind speeds that were confined to a height of less than 2 km AGL.

The LLJ events at RUTNJ were strong, with little respite between the LLJ and DW events. Both regimes showed comparable wind speeds, unlike BLTMD where the DW events were more intense. The LLJ events between the North Carolina sites were quite different. RALNC had a much stronger LLJ relative to CHANC, where the LLJ was virtually nonexistent. The LLJ appeared to be primarily modified by the local topography of the Fall Line while the DW was primarily controlled by the distance from the Appalachian Mountains.

d. *Regional WeatherBug network*

Regional surface observations were used to help further investigate the nocturnal regimes. WeatherBug data from the Earth Networks company, based in Germantown, Maryland, offered high-temporal-resolution surface observations from hundreds of stations in the mid-Atlantic region. Although previous literature has mentioned siting and calibration issues associated with this dataset (Hilliker et al. 2010), the focus of this research is on trends in wind speed and direction as opposed to measurement accuracy. Nevertheless, quality control measures were used to exclude sites that were spatially inconsistent with neighboring stations. Reporting stations were selected nearest to north–south, west–east, and northwest–southeast transects to explore the propagation of nocturnal patterns along different directions (see Fig. 1 for the station locations, labeled A–Q, along the west–east transect).

Figure 7 shows winds from WeatherBug sites A–Q (Fig. 1) for the nocturnal period of 2 August. We caution that not all WeatherBug sites equally demonstrate the nocturnal events due to their individual geographic locations or any possible obstructions located nearby. The propagation of a wind direction transition (denoted by a line labeled α) from southwesterly to northwesterly begins at approximately 2300 UTC in the Piedmont Plateau (station F) and continues until 1200 UTC along Maryland's Eastern Shore (site P). Wind speeds after

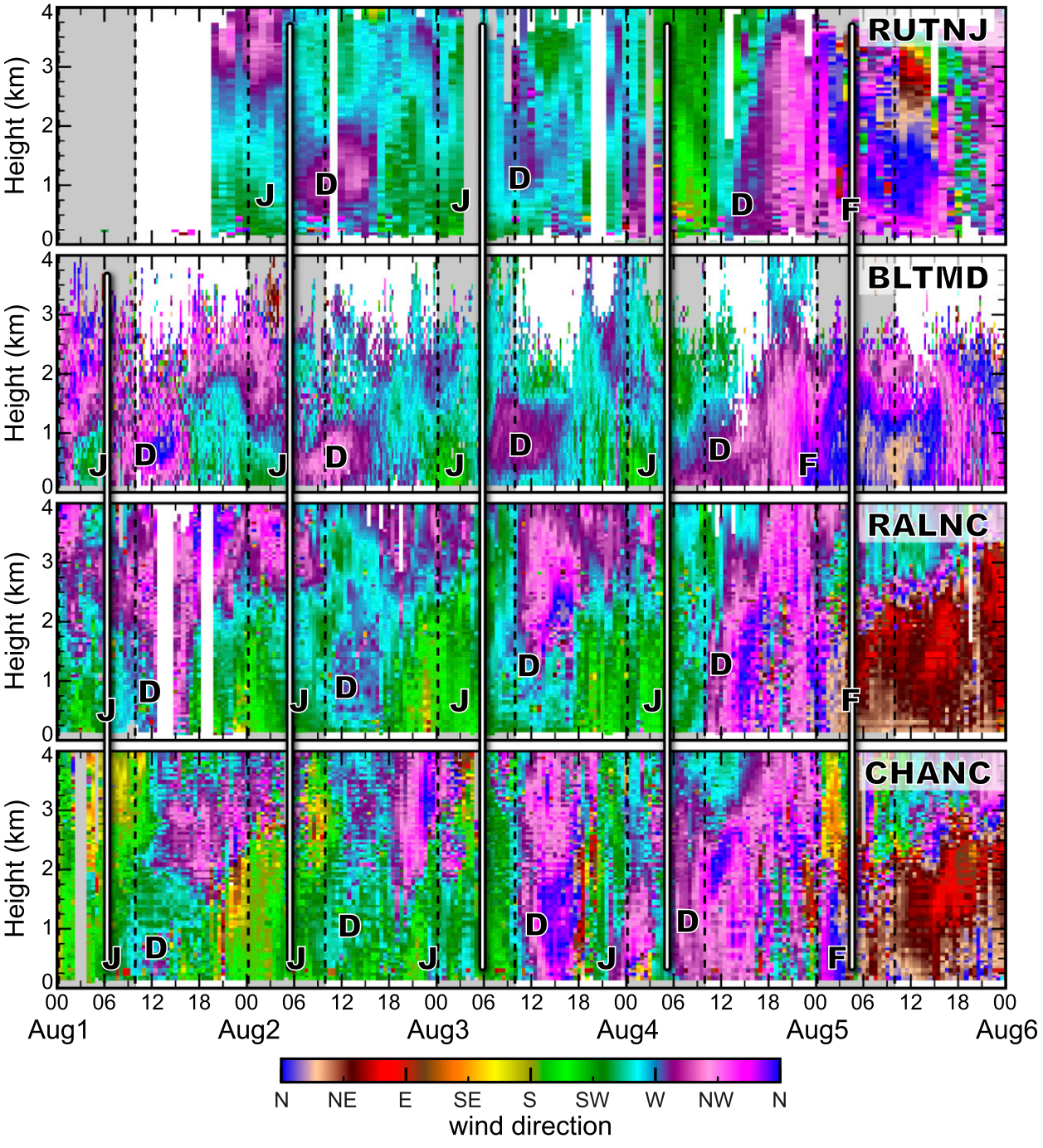

FIG. 5. Comparison of wind direction between wind profilers at (a) RUTNJ, (b) BLTMD, (c) RALNC, and (d) CHANC from 0000 UTC 1 Aug to 0000 UTC 6 Aug 2006 (see Fig. 1 for locations). White lines mark the beginning of the DW regime at HUBRC. Gray-shaded background indicates nighttime periods. Letters J, D, and F designate low-level jet, downslope winds, and cold-frontal events, respectively.

this transition remained relatively calm. The line labeled β shows the propagation of a wind speed increase. This period of a wind speed increase, primarily noticed starting at station H, is believed to be related to the most intense part of the DW air mass passing overhead, similar to strong winds that can follow the passage of a cold front. This timing coincides very well with the DW regime observed at site K near HUBRC. Wind data from the north–south transect that was located east of the Blue Ridge Mountains (not shown) revealed that the wind transitions first appeared in the Potomac River valley just north of sites G and H

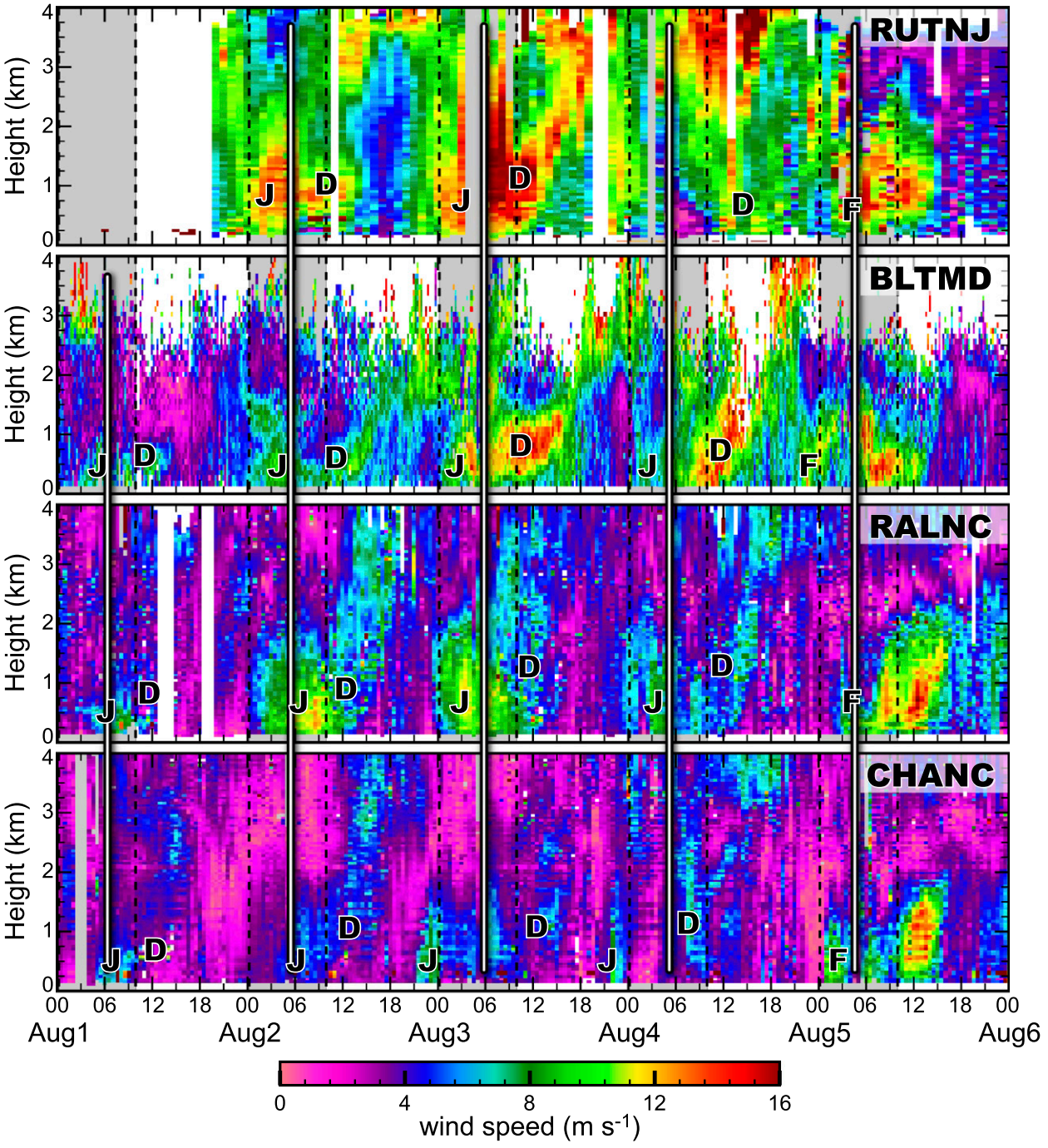

FIG. 6. As in Fig. 5, but for wind speed.

(Fig. 1) and then fanned out eastward from there. While these DW events are believed to be primarily driven by cross-barrier mountain flow dynamics, it is not unreasonable to assume that DW flows should respond to gravitational acceleration in a similar manor as traditional drainage flows (Sakiyama 1990) and preferentially follow the down-valley path of least resistance, in this case, a notch in the Blue Ridge Mountains (region 5 in Fig. 1) carved by the Potomac River. It is also reasonable to assume that nocturnal radiative cooling on these clear nights might have played some role in enhancing the DW intensity, especially relative to the warm moist coastal air mass to the east.

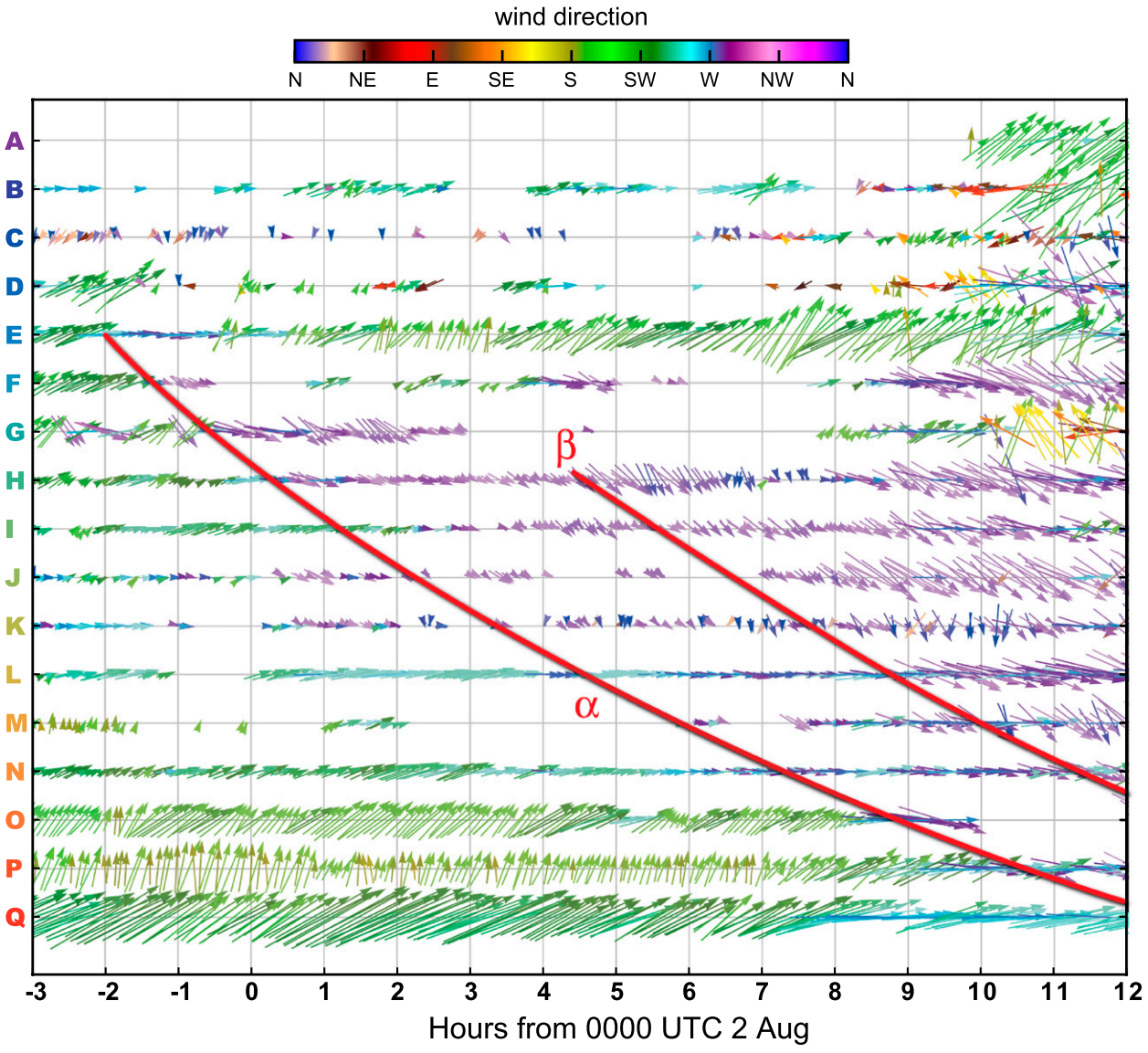

FIG. 7. WeatherBug surface wind observations from 2100 UTC 1 Aug to 1200 UTC 2 Aug 2006. Station sites are labeled A–Q and correspond to the locations in Fig. 1. Vectors are oriented with the wind flow. Two red lines are superimposed to delineate the nocturnal transitions that propagated from west to east. Line α marks the change in wind direction, and β marks the change in wind speed.

It is interesting to note that the DW event was most clearly observed by WeatherBug sites just north of Washington. It is conjectured that the DW flowed down the east flank of the Blue Ridge Mountains and, then, broadened out along the surface while moving eastward and moderating with distance. The Piedmont Plateau region just north of Washington is slightly raised in elevation and located directly downstream from the water gap in the Blue Ridge Mountains, which would be most exposed to any downslope winds that were present. It is further hypothesized that most WeatherBug stations west of the Blue Ridge did not reveal any DW characteristics because those sites were situated in somewhat narrow valleys with ridges oriented perpendicular to the DW flow, thereby isolating these stations from air motions aloft. These locational and surface roughness effects, when combined with nocturnal stability and a layered environment, could allow the DW to simply glide above the ribbed topography all the way from the Appalachian Highlands to the Blue Ridge Mountains without ever influencing surface observations in the narrow valleys.

5. Synthesis into a conceptual model

The cyclical pattern observed in the PBL during this case study is simplified here into a conceptual model to

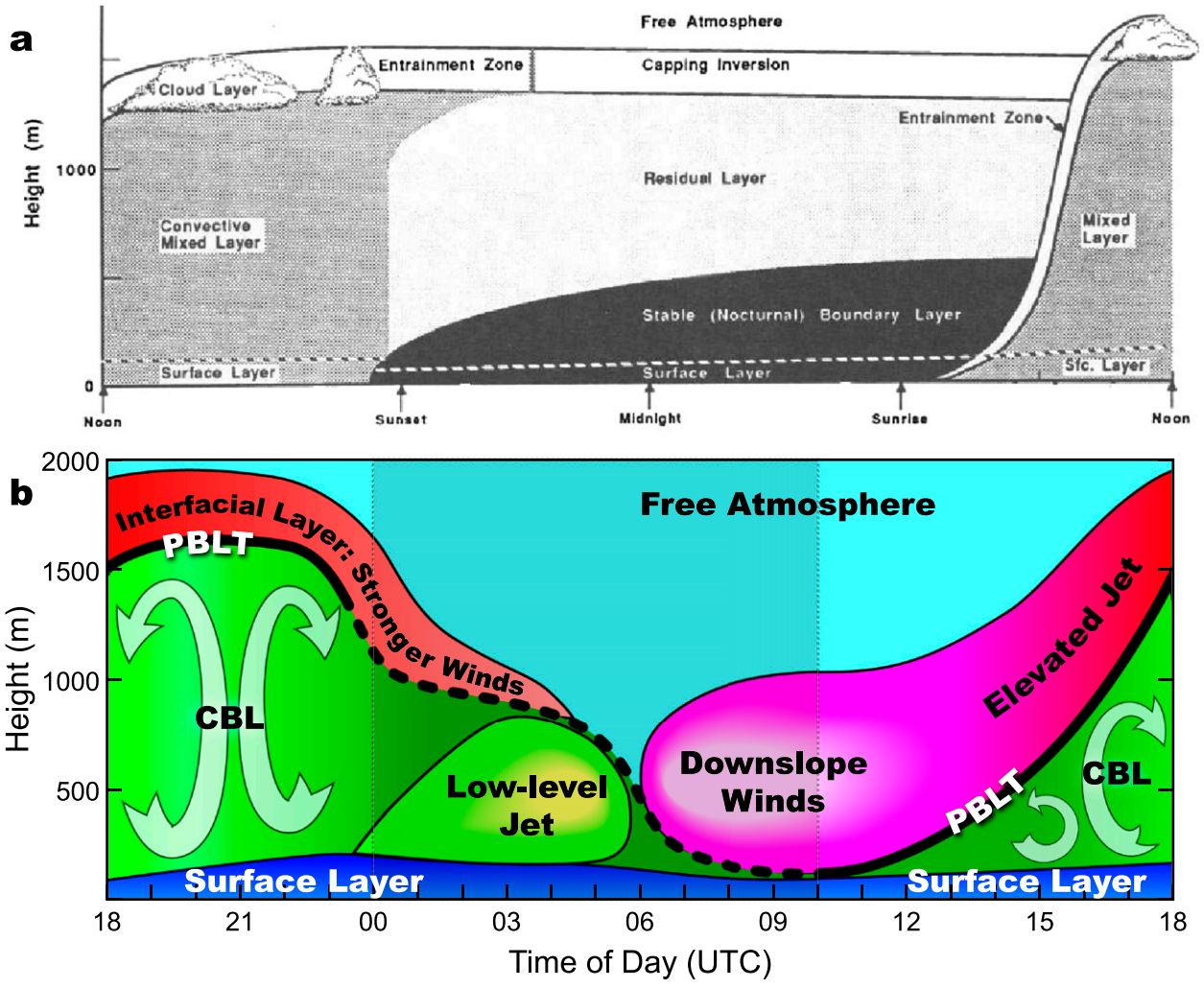

FIG. 8. Diurnal evolution of (a) the classic boundary layer depicted by Stull (1988) and (b) the modified conceptual model of PBL evolution at HUBRC based on case-study observations.

highlight the primary mechanisms that are responsible for the observed prefrontal environment in the mid-Atlantic region and to more easily identify similar patterns in the future.

The three-stage diurnal pattern

Measurements acquired during this case study are indicative of mesoscale processes not illustrated in the conceptual PBL model of Stull (1988) in Fig. 8a. This is a good teaching model that is best realized for idealized PBL patterns on clear, calm days over flat terrain. However, it does not account for PBL alterations over complex terrain (Bader and McKee 1992; Kumar et al. 2012; Seaman et al. 2012), urban effects (Godowitch et al. 1985; Martilli 2002), coastal regions (Haman et al. 2012), synoptic forcings (Gopalakrishnan et al. 1998; Rama Krishna et al. 2003), or other local perturbations of the PBL. In the mid-Atlantic region, there are often complex interactions between topography and the thermal gradients that can induce low-level flows that modify the idealized PBL evolution.

A modified depiction of the diurnal cycle is presented in Fig. 8b, which more closely represents the interplay between wind regimes that were observed during the prefrontal period of this case study. This modified diurnal cycle can be simplified into three stages: (i) daytime CBL development, (ii) partial collapse of the PBL near sunset with an intensification of low-level flows leading to LLJ development, and (iii) airmass displacement by the DW. Figure 8b is meant to expound upon Stull's original illustration in order to better communicate the similarities and differences in the PBL evolution for the mid-Atlantic region under similar synoptic patterns. A cursory examination of the BLTMD

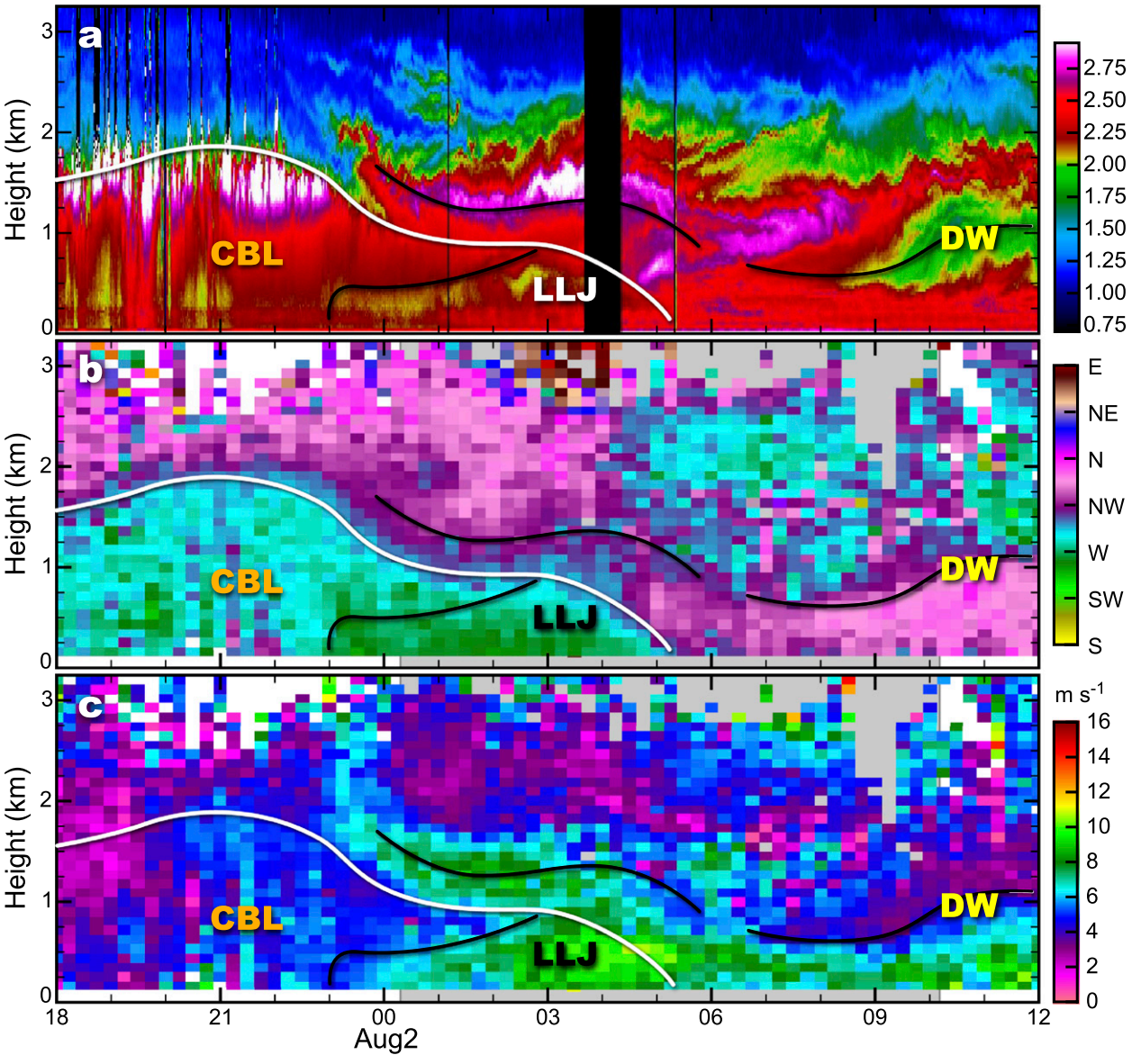

FIG. 9. Enlargement of nocturnal phenomena from 1800 UTC 1 Aug to 1200 UTC 2 Aug 2006. Shown are (a) ASR, (b) wind direction, and (c) wind speed. Collocated lines are superimposed onto each panel as a visual aid to help identify common features among fields. The white line is the hypothesized PBLT.

wind profiler data suggests this diurnal pattern was not unique to this case study alone, but often occurs throughout the year, and can persist for multiple days in a row.

It should be emphasized that it is a challenging endeavor to discern the evolutionary structures and height of the late day or nocturnal PBLs. During these times, vertical gradients of moisture and ASR that distinguish the PBL from the free atmosphere are more subtle and diffuse compared to the starker contrasts that are usually observed during the daytime CBL. In the absence of a thermal time series during this case study, the PBL top (PBLT) was estimated by overlaying wind and lidar time series imagery and by identifying collocated heights showing more pronounced gradients. For example, contrasts between the ASR values within the CBL and the cleaner air above it were useful for estimating the PBLT. A change in wind speed or direction with height was another useful indicator for distinguishing a possible PBLT. The wind profiler signal-to-noise ratio (SNR) was also used to help determine appropriate PBLT placement, because the SNR values are related to beam refraction, which occurs where there are moisture or temperature gradients, such as inversion layers or

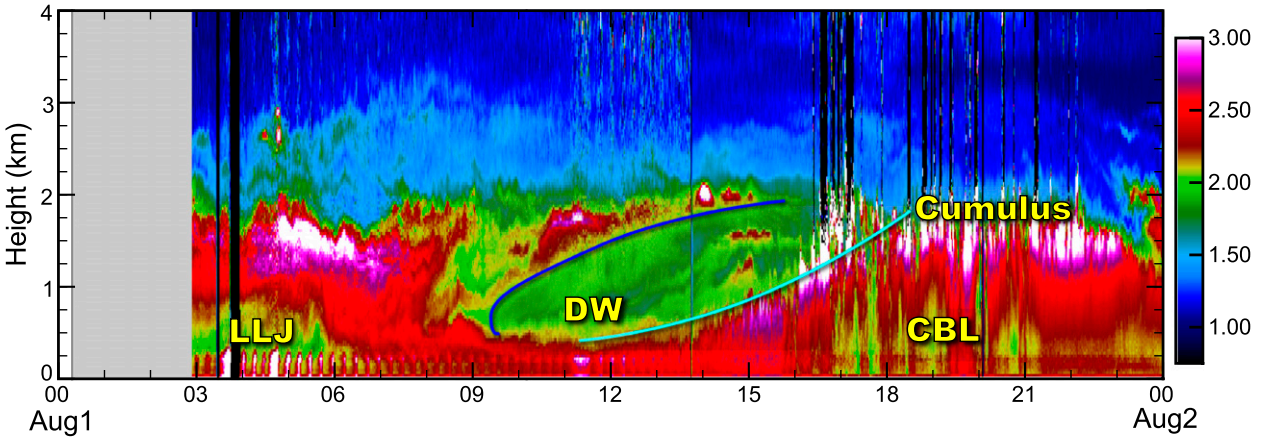

FIG. 10. Enlargement of Fig. 3b showing ASR data for 1 Aug. Important features are labeled. The blue line shows lifting by the DW, and the cyan line traces the top of the developing CBL.

entrainment zones. Therefore, our observational approach was to synthesize all of the above observations in defining a PBLT, rather than to depend on any single field by itself. Locations of the PBLT, dashed in Fig. 8b, indicate some height uncertainty in the dataset.

The PBL structures presented here show several, mostly nocturnal, differences from the classic Stull model (cf. Figs. 8a and 8b). Unlike the classic PBL, the first half of each night was characterized by the building of an LLJ regime, and the second half by the DW regime. Another difference was that the upper portion of the CBL did not appear to decouple in the same manner as in the idealized model, around sunset, and then gradually fade into a residual layer. Instead, an interfacial layer with higher wind speeds slowly descended during the early nighttime period. The descent was likely due to the diminishing daytime convection and an environment characterized by subsidence under a high pressure area. We estimated that the PBLT followed the height of the interfacial layer during the late day period (Fig. 8b) because the atmosphere below was still relatively homogeneous down to the surface, as compared to the atmosphere above it, thus exhibiting significantly different characteristics. This was most evident in the wind direction field (Fig. 9b). Our PBLT estimation over this period was different from Stull's (Fig. 8a), which infers a discontinuous PBLT that abruptly stops following the top of the CBL, then reappears near the surface tracing the growth of the stable nocturnal boundary layer (SBL). In our case, we did not observe a well-defined SBL. Concurrent with the falling PBLT during the evening period, near-surface wind speeds began to increase and expand upward as part of the LLJ development. Eventually, the top of the LLJ and the descending layer of interfacial winds intersected. At that point, the rate that the PBLT had been lowering slowed down while the LLJ regime strengthened below it. This continued until the arrival of the DW, which displaced the LLJ regime and eroded its characteristics all the way down to the surface layer. Within the surface layer, however, winds still remained southwesterly (Fig. 4b). For this reason, we estimated that the PBLT was most appropriately located below the DW regime since near-surface conditions were very different from those ~100 m above the surface.

1) STAGE I: CONVECTIVE BOUNDARY LAYER

The growth of the CBL began with sunrise, shortly after 1100 UTC each day, and continued until about 1600 UTC. This period of CBL growth is denoted with a cyan line in Fig. 10 above a layer of higher ASR values that rise from 400 m to 1.7 km and characterize the CBL. ASR values often peak near the top of the CBL due to the larger effective radius of particulates from hygroscopic growth in air with higher relative humidity. The air above the CBL tends to be cleaner due to diffusion by stronger winds aloft, which usually advects particulates away from sources in the lower atmosphere. Therefore, the ASR data show a clear gradient denoting the top of a growing or mature CBL. From 1600 to 2200 UTC, the CBL maintained a maximum height of approximately 1.7 km AGL. Very high ASR values (1500–2300 UTC) at the top of this layer indicated the presence of cumulus clouds. The afternoon CBL on 1–3 August was characterized by light west-southwest winds from ~1700 UTC until dusk (Fig. 3c). The prefrontal mixing ratio within the PBL remained roughly uniform at 15–16 g kg^{-1} (Fig. 3a).

2) STAGE II: NOCTURNAL LOW-LEVEL JET REGIME

Figure 9 is an enlargement of the ASR and wind data from 1800 UTC 1 August to 1200 UTC 2 August shown

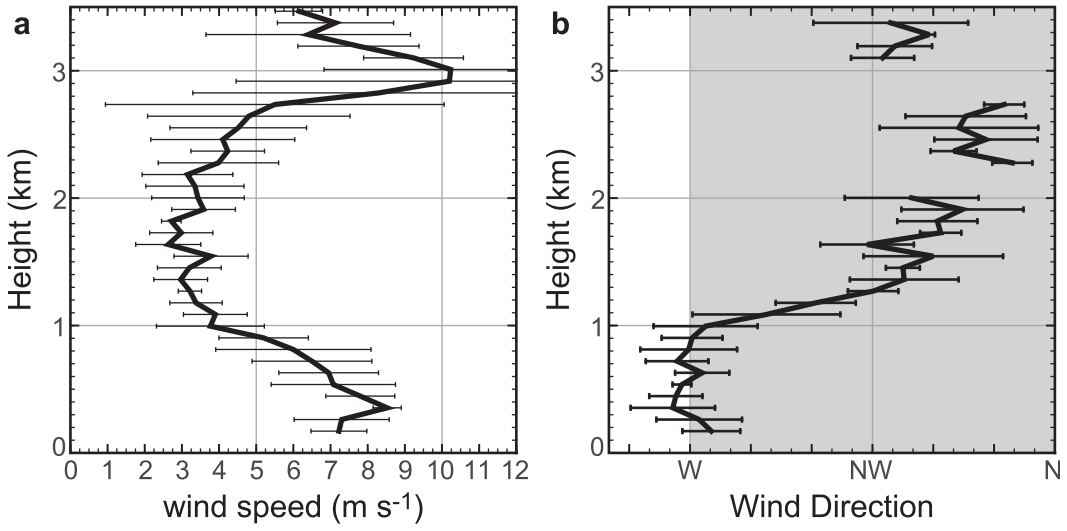

FIG. 11. LLJ observed by the MDE wind profiler showing wind (a) speed and (b) direction from 0430 to 0545 UTC 1 Aug. Northwest quadrant of the wind direction is shaded gray.

in Fig. 3. This day was representative of the prefrontal diurnal pattern presented in Fig. 8, and provides a more detailed view of the nocturnal stages and transitions between them. The juxtapositional analysis of ASR, wind speed, and wind direction data provides a powerful diagnostic for inferring nocturnal structure and flow. It is reasonable to place the initiation of the PBL collapse about 2 h prior to sunset (2200 UTC), when the locations with highest ASR values (Fig. 9a) started decreasing in altitude. Scattered cumulus clouds, indicated by high ASR values at 1.7 km, began dissipating after 2300 UTC. As previously mentioned, from 2200 to 0300 UTC higher winds associated with an interfacial layer began to lower in altitude from ~2.5 to 1.0 km (Fig. 9c). It is unclear whether the increasing interfacial winds are a precursor to the DW building aloft, or whether it is a different phenomenon altogether, since both have a northwesterly flow. More research is needed to understand this situation. Preferably, this research would include cases when the wind profiler data extend higher above the PBL. Regardless, the LLJ regime appears to originate from the surface and progress upward on all four prefrontal nights and, thus, is somewhat decoupled from the dynamics above.

Figure 11 shows a representative LLJ wind profile from 1 August at HUBRC. This was the weakest LLJ regime of the four prefrontal nights. On this night the wind direction tended to a more westerly than southwesterly direction but abruptly shifted to the northwest above 1 km. The wind speed exhibited a classic nose profile, with positive shear below the core and negative shear above it (Fig. 11a). Overall, the LLJ regimes on 1–4 August had core wind speeds of 9, 11, 14, and 9 m s^{-1} located at 350, 500, 500, and 400 m AGL, respectively. The vertical zone of negative shear above the LLJ is referred to as the wind speed falloff region. Wind speed falloff values averaged 5, 6, 6, and 4 m s^{-1} on 1–4 August, respectively. This corresponds to at least a 40% reduction of wind speed above the jet core. These attributes are more than sufficient to qualify as an LLJ, according to Baas et al. (2009). The wind direction tended to have an increasingly southern component each night ahead of the cold front. The depth of the LLJ regime was shallow, below 1 km, and peak winds remained close to the surface. The LLJ regimes in this case study sustained maximum wind speeds for a period of roughly 2–3 h. The timing of the most intense wind speeds (0100–0430 UTC) was a bit earlier than expected, according to the timing of the normal inertial oscillation cycle expected at HUBRC. Theoretically, winds should peak closer to 0600–0700 UTC. It is conjectured that the DW regime during this case study interrupts the LLJ regime, which might otherwise have kept intensifying.

3) STAGE III: DOWNSLOPE WIND REGIME

The most striking features in the ASR fields were regions of elevated cleaner air (ECA) that appeared during 1–4 August (labeled D in Fig. 3b). These ECAs appeared each day between 0600 and 0800 UTC, well before dawn. HUBRC temperature soundings at 0655 UTC 1 August and 1044 UTC 3 August (not shown) showed an inversion located at 150–200 m AGL, which was estimated to be the SBL top. The ECA regions penetrated down to 500 m AGL on 1–2 August, but extended beyond the lowest wind profiler level (175 m), and presumably down to the SBL, on 3–4 August. These

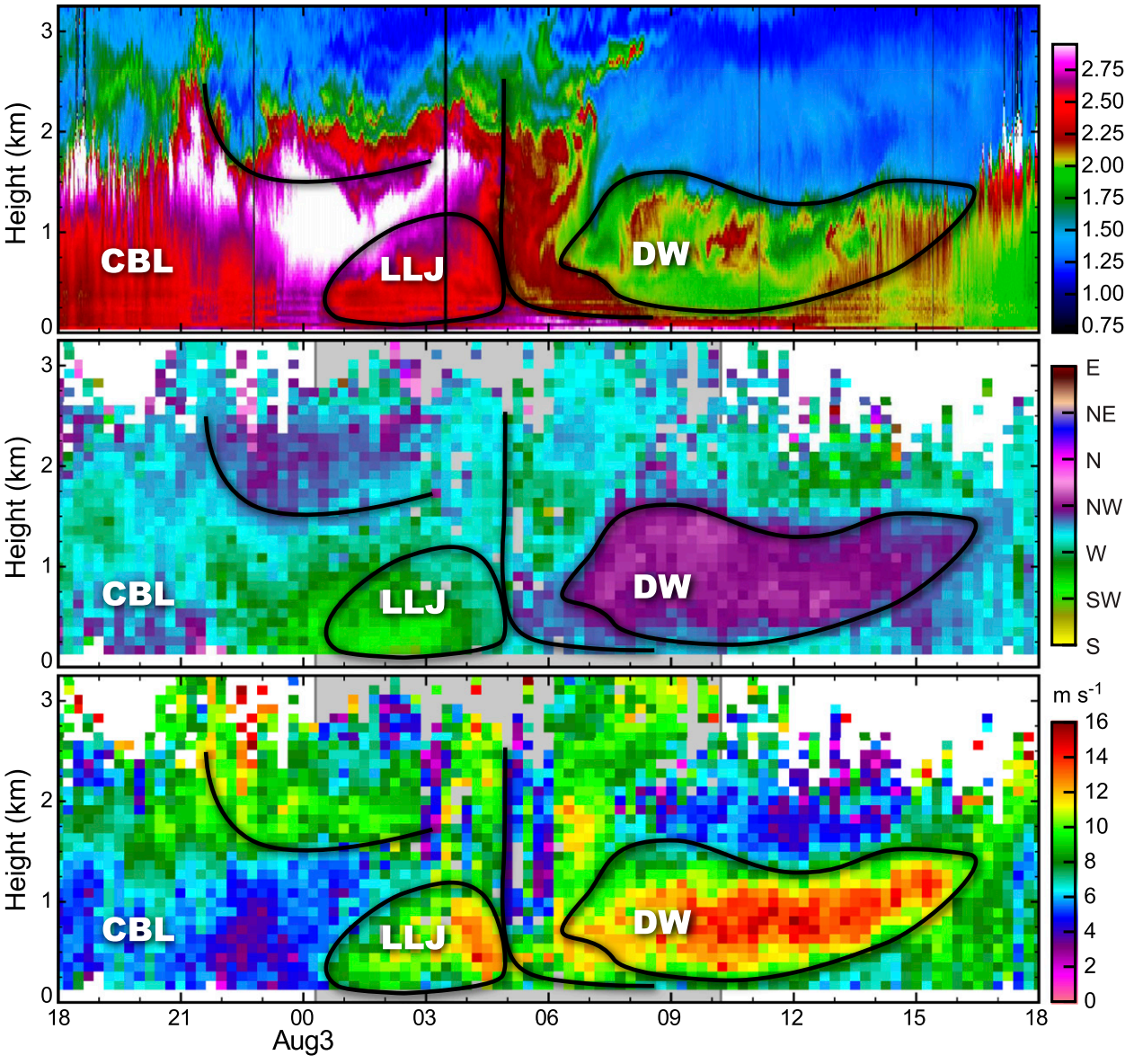

FIG. 12. As in Fig. 9, but from 1800 UTC 2 Aug to 1800 UTC 3 Aug.

ECA regions were associated with a change to a northwesterly wind direction and a simultaneous increase in wind speed that continued beyond dawn. The DW during the nights of 1–2 August showed that the strongest winds were located just above the SBL (175–500 m); while the core of the DW (500–2000 m), indicated by the clearing in the ASR data, was characterized by relatively calm wind speeds (Fig. 9). By contrast, the nights of 3 and 4 August showed that the maximum wind speeds were located in the DW core (400–1200 m) with a more pronounced clearing of the ASR field (Fig. 12). In all four of the cases, the wind direction was the principal indicator of a regime change.

The data indicate that the DW displaced the existing air mass associated with the LLJ phenomenon in the lowest 1.5 km. While horizontal advective processes dominated the DW core, it is speculated that the secondary effect was to gradually lift the layer of southwesterly flow throughout the remainder of the night and into the daylight hours. In the absence of vertical wind measurements, air with higher ASR values was used as a tracer for atmospheric motion. This is best realized by examining the strongest DW event on 4 August. ASR measurements (Fig. 13) revealed a large borelike curl (red-shaded values), indicating possible horizontal vorticity in the lowest kilometer, during 0600–0730 UTC.

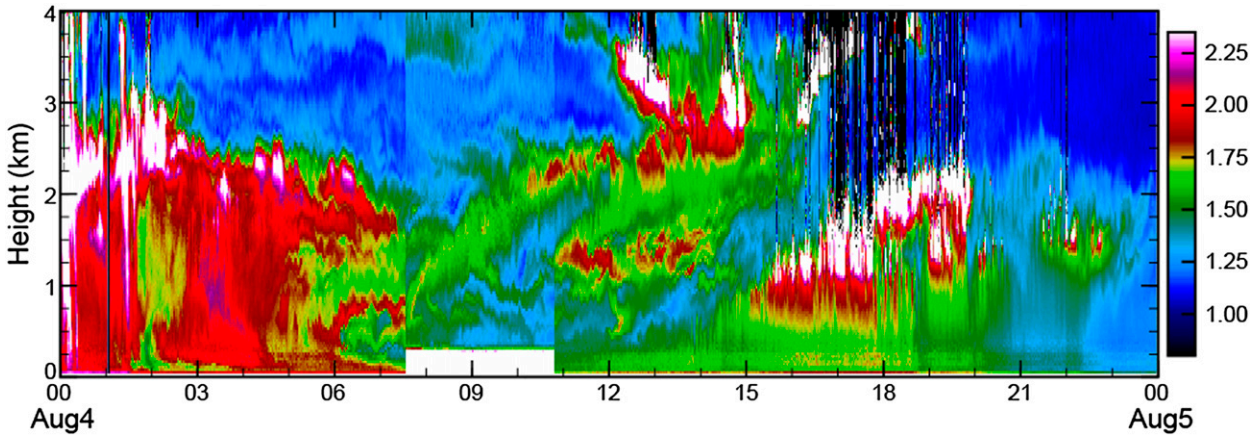

FIG. 13. Enlargement of Fig. 3b showing ASR data on 4 Aug. The DW event was greatly enhanced by the prefrontal trough in comparison with previous days.

The passage of this DW nose resulted in both horizontal and vertical airmass displacement at 0600 UTC, although a close examination of the data showed hints of displacement starting as early as 0400 UTC. Areas indicating strong lifting were evident by a band of increased ASR values that lifted from 0.5 to 2.5 km between 0700 and 1200 UTC (yellow-to-red-shaded values). The lidar profile time series revealed some similarities between the structure of the DW events and density currents (Geerts et al. 2006). For example, all DW events had a clearly defined nose, and the events of 2–3 August showed a more well-defined head region, similar to density current features. Furthermore, ASR data were used as a tracer that displayed visual evidence of turbulent mixing in the wake region. A significant difference between the two, however, was that the onset of daytime heating and CBL development tended to curtail what might have developed into a longer DW body region.

6. Concluding remarks

In this study, measurements from the WAVES 2006 field campaign and the other available data are used to examine some intriguing cyclical low-level flows during the prefrontal period over the mid-Atlantic region with complex geography. Results showed a distinct diurnal pattern during the prefrontal period of this case study, which can be categorized into three stages: (i) growth and decay of the CBL, (ii) development of an LLJ regime, and (iii) disruption by a DW regime. This three-stage model highlights important differences from the ideal depiction of the nocturnal boundary layer, which does not account for low-level winds induced by complex geography. The CBL regime in stage I was characterized by northwesterly flow with wind speeds that diminished and veered southwesterly by late afternoon. Stage II began near sunset when the PBL collapsed to half its height and subkilometer wind speeds intensified into an LLJ that was oriented parallel to the mountains. Stage III occurred midway through the nighttime when stronger northwesterly winds, which were oriented perpendicular to and originating from the Appalachian Mountains, displaced the LLJ regime.

This research has emphasized the importance of a holistic analytical approach to low-level wind observations, discriminating between low-level wind speed maxima based on airmass properties and origin. At first glance, the wind speed profiles of the DW regime were very similar in appearance to those of LLJs. However, the wind direction between them is 90° out of phase. Furthermore, there is a significant difference in ASR between the two air masses. Therefore, the DW should be realized as a separate phenomenon apart from the classic notion of an LLJ by taking into consideration wind direction and other airmass properties.

Another important contribution of this work is the influence and detection of the DW as far downstream from the Appalachian Mountains as the greater Baltimore–Washington metropolitan area. This research demonstrates how low-profile mountain ranges can still generate weaker DW events that can affect and disrupt local meteorology, circulations, or existing wind regimes, such as the LLJ. Such changes in low-level winds during the nocturnal period would undoubtedly impact air quality forecasts, which typically presume an idealized nocturnal PBL evolution pattern. Furthermore, the processes of atmospheric chemistry strongly depend upon assumptions regarding the nocturnal boundary layers, turbulence characteristics, and the prevailing wind direction with

respect to pollution sources. There has been an increased focus on how LLJ events modify such processes, but little discussion on how interruptions by DW events could modify these processes in the mid-Atlantic region. The PBL model presented in this research may provide additional insight into anomalous or discontinuous air quality observations throughout the nocturnal period that may be associated with the concept of a split wind regime.

Since the wind profile time series data were only available at a few limited sites, it is not possible to examine the full three-dimensional structure and the associated dynamics of the nocturnal LLJ and DW regimes. Future research will investigate the temporal and spatial patterns of evolution of these low-level flows through numerical simulations. Additionally, research efforts should examine the climatology of similar diurnal patterns using existing observational datasets, and compare the synoptic variance under which these events evolve in order to assess the impact to air quality forecasts.

Acknowledgments. This research was funded under the NASA Atmospheric Composition Program and occurred within the NASA GSFC Mesoscale Atmospheric Processes Laboratory. We acknowledge the Aura Validation project for funding the WAVES campaign. We thank Howard University and the Maryland Department of the Environment for use of their instrument data.

REFERENCES

Adam, M., and Coauthors, 2010: Water vapor measurements by Howard University Raman lidar during the WAVES 2006 campaign. *J. Atmos. Oceanic Technol.,* **27,** 42–60, doi:10.1175/2009JTECHA1331.1.

Andreas, E. L, K. J. Claffy, and A. P. Makshtas, 2000: Low-level atmospheric jets and inversions over the western Weddell Sea. *Bound.-Layer Meteor.,* **97,** 459–486, doi:10.1023/A:1002793831076.

Baas, P., F. C. Bosveld, H. K. Baltink, and A. A. M. Holtslag, 2009: A climatology of nocturnal low-level jets at Cabauw. *J. Appl. Meteor. Climatol.,* **48,** 1627–1642, doi:10.1175/2009JAMC1965.1.

Bader, D. C., and T. B. McKee, 1992: Mesoscale boundary-layer evolution over complex terrain. Part II: Factors controlling nocturnal boundary-layer structure. *Mon. Wea. Rev.,* **120,** 802–816, doi:10.1175/1520-0493(1992)120<0802:MBLEOC>2.0.CO;2.

Banta, R. M., R. K. Newsom, J. K. Lundquist, Y. L. Pichugina, R. L. Coulter, and L. Mahrt, 2002: Nocturnal low-level jet characteristics over Kansas during CASES-99. *Bound.-Layer Meteor.,* **105,** 221–252, doi:10.1023/A:1019992330866.

Blackadar, A. K., 1957: Boundary layer wind maxima and their significance for the growth of nocturnal inversions. *Bull. Amer. Meteor. Soc.,* **38,** 283–290.

Blier, W., 1998: The sundowner winds of Santa Barbara, California. *Wea. Forecasting,* **13,** 702–716, doi:10.1175/1520-0434(1998)013<0702:TSWOSB>2.0.CO;2.

Bonner, W. D., 1968: Climatology of the low level jet. *Mon. Wea. Rev.,* **96,** 833–850, doi:10.1175/1520-0493(1968)096<0833:COTLLJ>2.0.CO;2.

Brinkmann, W. A. R., 1974: Strong downslope winds at Boulder, Colorado. *Mon. Wea. Rev.,* **102,** 592–602, doi:10.1175/1520-0493(1974)102<0592:SDWABC>2.0.CO;2.

Colle, B. A., and C. F. Mass, 1998: Windstorms along the western side of the Washington Cascade Mountains. Part I: A high-resolution observational and modeling study of the 12 February 1995 event. *Mon. Wea. Rev.,* **126,** 28–52, doi:10.1175/1520-0493(1998)126<0028:WATWSO>2.0.CO;2.

——, and D. R. Novak, 2010: The New York Bight jet: Climatology and dynamical evolution. *Mon. Wea. Rev.,* **138,** 2385–2404, doi:10.1175/2009MWR3231.1.

Colman, B. R., and C. F. Dierking, 1992: The taku wind of southeast Alaska: Its identification and prediction. *Wea. Forecasting,* **7,** 49–64, doi:10.1175/1520-0434(1992)007<0049:TTWOSA>2.0.CO;2.

Decker, S. G., and D. A. Robinson, 2011: Unexpected high winds in northern New Jersey: A downslope windstorm in modest topography. *Wea. Forecasting,* **26,** 902–921, doi:10.1175/WAF-D-10-05052.1.

Delgado, R., S. D. Rabenhorst, B. B. Demoz, and R. M. Hoff, 2014: Elastic lidar measurements of summer nocturnal low level jet events over Baltimore, Maryland. *J. Atmos. Chem.,* doi:10.1007/s10874-013-9277-2, in press.

Durran, D. R., 2003: Downslope winds. *Encyclopedia of Atmospheric Sciences,* J. R. Holton, J. Pyle, and J. A. Curry, Eds., Elsevier, 1161–1170.

Ferrare, R., and Coauthors, 2006: Evaluation of daytime measurements of aerosols and water vapor made by an operational Raman lidar over the southern Great Plains. *J. Geophys. Res.,* **111,** D05S08, doi:10.1029/2005JD005836.

Gaffin, D. M., 2009: On high winds and foehn warming associated with mountain-wave events in the western foothills of the southern Appalachian Mountains. *Wea. Forecasting,* **24,** 53–75, doi:10.1175/2008WAF2007096.1.

Geerts, B., R. Damiani, and S. Haimov, 2006: Finescale vertical structure of a cold front as revealed by an airborne Doppler radar. *Mon. Wea. Rev.,* **134,** 251–271, doi:10.1175/MWR3056.1.

Godowitch, J. M., J. K. S. Ching, and J. F. Clarke, 1985: Evolution of the nocturnal inversion layer at an urban and nonurban location. *J. Climate Appl. Meteor.,* **24,** 791–804, doi:10.1175/1520-0450(1985)024<0791:EOTNIL>2.0.CO;2.

Goldsmith, J. E. M., F. H. Blair, S. E. Bisson, and D. D. Turner, 1998: Turn-key Raman lidar for profiling atmospheric water vapor, clouds, and aerosols. *Appl. Opt.,* **37,** 4979–4990, doi:10.1364/AO.37.004979.

Gopalakrishnan, S. G., M. Sharan, R. T. McNider, and M. P. Singh, 1998: Study of radiative and turbulent processes in the stable boundary layer under weak wind conditions. *J. Atmos. Sci.,* **55,** 954–960, doi:10.1175/1520-0469(1998)055<0954:SORATP>2.0.CO;2.

Grisogono, B., and D. Belušić, 2009: A review of recent advances in understanding the meso- and microscale properties of the severe bora wind. *Tellus,* **61A,** 1–16, doi:10.1111/j.1600-0870.2008.00369.x.

Grubisic, V., and M. Xiao, 2006: Climatology of westerly wind events in the lee of the Sierra Nevada. Preprints, *12th Conf. on Mountain Meteorology,* Santa Fe, NM, Amer. Meteor. Soc., P2.8. [Available online at https://ams.confex.com/ams/pdfpapers/114755.pdf.]

Haman, C. L., B. Lefer, and G. A. Morris, 2012: Seasonal variability in the diurnal evolution of the boundary layer in a near coastal urban environment. *J. Atmos. Oceanic Technol.,* **29,** 697–710, doi:10.1175/JTECH-D-11-00114.1.

Hilliker, J. L., G. Akasapu, and G. S. Young, 2010: Assessing the short-term forecast capability of nonstandardized surface observations using the National Digital Forecast Database (NDFD). *J. Appl. Meteor. Climatol.,* **49,** 1397–1411, doi:10.1175/2010JAMC2137.1.

Holton, J. R., 1967: The diurnal boundary layer wind oscillation above sloping terrain. *Tellus,* **19,** 199–205, doi:10.1111/j.2153-3490.1967.tb01473.x.

Jiang, X., N.-C. Lau, I. M. Held, and J. J. Ploshay, 2007: Mechanisms of the Great Plains low-level jet as simulated in an AGCM. *J. Atmos. Sci.,* **64,** 532–547, doi:10.1175/JAS3847.1.

Jones, H. G., 1983: *Plants and Microclimate: A Quantitative Approach to Environmental Physiology.* Cambridge University Press, 323 pp.

Karipot, A., M. Y. Leclerc, and G. Zhang, 2009: Characteristics of nocturnal low-level jets observed in the north Florida area. *Mon. Wea. Rev.,* **137,** 2605–2621, doi:10.1175/2009MWR2705.1.

Klemp, J. B., and D. R. Lilly, 1975: The dynamics of wave-induced downslope winds. *J. Atmos. Sci.,* **32,** 320–339, doi:10.1175/1520-0469(1975)032<0320:TDOWID>2.0.CO;2.

Koletsis, I., K. Lagouvardos, V. Kotroni, and A. Bartzokas, 2009: Numerical study of a downslope windstorm in northwestern Greece. *Atmos. Res.,* **94,** 178–193, doi:10.1016/j.atmosres.2009.05.012.

Kumar, M. S., V. K. Anandan, T. N. Rao, and P. N. Reddy, 2012: A climatological study of the nocturnal boundary layer over a complex-terrain station. *J. Appl. Meteor. Climatol.,* **51,** 813–825, doi:10.1175/JAMC-D-11-047.1.

Martilli, A., 2002: Numerical study of urban impact on boundary layer structure: Sensitivity to wind speed, urban morphology, and rural soil moisture. *J. Appl. Meteor.,* **41,** 1247–1266, doi:10.1175/1520-0450(2002)041<1247:NSOUIO>2.0.CO;2.

Melfi, S. H., D. Whiteman, and R. Ferrare, 1989: Observation of atmospheric fronts using Raman lidar moisture measurements. *J. Appl. Meteor.,* **28,** 789–806, doi:10.1175/1520-0450(1989)028<0789:OOAFUR>2.0.CO;2.

Meyers, M. P., J. S. Snook, D. A. Wesley, and G. S. Poulos, 2003: A Rocky Mountain storm. Part II: The forest blowdown over the west slope of the northern Colorado mountains—Observations, analysis, and modeling. *Wea. Forecasting,* **18,** 662–674, doi:10.1175/1520-0434(2003)018<0662:ARMSPI>2.0.CO;2.

Nkemdirim, L. C., 1986: Chinooks in southern Alberta: Some distinguishing nocturnal features. *J. Climatol.,* **6,** 593–603, doi:10.1002/joc.3370060603.

Parish, T. R., and L. D. Oolman, 2010: On the role of sloping terrain in the forcing of the Great Plains low-level jet. *J. Atmos. Sci.,* **67,** 2690–2699, doi:10.1175/2010JAS3368.1.

——, A. R. Rodi, and R. D. Clark, 1988: A case study of the summertime Great Plains low level jet. *Mon. Wea. Rev.,* **116,** 94–105, doi:10.1175/1520-0493(1988)116<0094:ACSOTS>2.0.CO;2.

Rama Krishna, T. B. P. S. R., M. Sharan, S. G. Gopalakrishnan, and Aditi, 2003: Mean structure of the nocturnal boundary layer under strong and weak wind conditions: EPRI case study. *J. Appl. Meteor.,* **42,** 952–969, doi:10.1175/1520-0450(2003)042<0952:MSOTNB>2.0.CO;2.

Raphael, M. N., 2003: The Santa Ana winds of California. *Earth Interact.,* **7,** doi:10.1175/1087-3562(2003)007<0001:TSAWOC>2.0.CO;2.

Rife, D. L., J. O. Pinto, A. J. Monaghan, C. A. Davis, and J. R. Hannan, 2010: Global distribution and characteristics of diurnally varying low-level jets. *J. Climate,* **23,** 5041–5064, doi:10.1175/2010JCLI3514.1.

Ryan, W. F., and Coauthors, 1998: Pollutant transport during a regional O_3 episode in the mid-Atlantic states. *J. Air Waste Manage. Assoc.,* **48,** 786–797, doi:10.1080/10473289.1998.10463737.

Sakiyama, S. K., 1990: Drainage flow characteristics and inversion breakup in two Alberta mountain valleys. *J. Appl. Meteor.,* **29,** 1015–1030, doi:10.1175/1520-0450(1990)029<1015:DFCAIB>2.0.CO;2.

Schultz, D. M., 2005: A review of cold fronts with prefrontal troughs and wind shifts. *Mon. Wea. Rev.,* **133,** 2449–2472, doi:10.1175/MWR2987.1.

Seaman, N. L., B. J. Gaudet, D. R. Stauffer, L. Mahrt, S. J. Richardson, J. R. Zielonka, and J. C. Wyngaard, 2012: Numerical prediction of submesoscale flow in the nocturnal stable boundary layer over complex terrain. *Mon. Wea. Rev.,* **140,** 956–977, doi:10.1175/MWR-D-11-00061.1.

Seluchi, M. E., F. A. Norte, P. Satyamurty, and S. C. Chou, 2003: Analysis of three situations of the foehn effect over the Andes (zonda wind) using the Eta–CPTEC regional model. *Wea. Forecasting,* **18,** 481–501, doi:10.1175/1520-0434(2003)18<481:AOTSOT>2.0.CO;2.

Sjostedt, D. W., J. T. Sigmon, and S. J. Colucci, 1990: The Carolina nocturnal low-level jet: Synoptic climatology and a case study. *Wea. Forecasting,* **5,** 404–415, doi:10.1175/1520-0434(1990)005<0404:TCNLLJ>2.0.CO;2.

Smith, C. M., and E. D. Skyllingstad, 2009: Investigation of upstream boundary layer influence on mountain wave breaking and lee wave rotors using a large-eddy simulation. *J. Atmos. Sci.,* **66,** 3147–3164, doi:10.1175/2009JAS2949.1.

——, and ——, 2011: Effects of inversion height and surface heat flux on downslope windstorms. *Mon. Wea. Rev.,* **139,** 3750–3764, doi:10.1175/2011MWR3619.1.

Song, J., K. Liao, R. L. Coulter, and B. M. Lesht, 2005: Climatology of the low-level jet at the southern Great Plains atmospheric boundary layer experiments site. *J. Appl. Meteor.,* **44,** 1593–1606, doi:10.1175/JAM2294.1.

Stull, R. B., 1988: *An Introduction to Boundary Layer Meteorology.* Kluwer Academic, 666 pp.

Turner, D. D., W. F. Feltz, and R. A. Ferrare, 2000: Continuous water vapor profiles from operational ground-based active and passive remote sensors. *Bull. Amer. Meteor. Soc.,* **81,** 1301–1317, doi:10.1175/1520-0477(2000)081<1301:CWBPFO>2.3.CO;2.

Verghese, S. J., S. N. Kizhakkemadam, A. Willitsford, J. P. Collier, S. Unni, and C. R. Philbrick, 2003: Characterization of nocturnal jets over Philadelphia during air pollution episodes. Preprints, *Fifth Conf. on Atmospheric Chemistry,* Long Beach, CA, Amer. Meteor. Soc., 6.10. [Available online at https://ams.confex.com/ams/pdfpapers/57487.pdf.]

Whiteman, C. D., and X. Bian, 1996: Solar semidiurnal tides in the troposphere: Detection by radar profilers. *Bull. Amer. Meteor. Soc.,* **77,** 529–542, doi:10.1175/1520-0477(1996)077<0529:SSTITT>2.0.CO;2.

——, ——, and S. Zhong, 1997: Low-level jet climatology from enhanced rawinsonde observations at a site in the southern Great Plains. *J. Appl. Meteor.,* **36,** 1363–1376, doi:10.1175/1520-0450(1997)036<1363:LLJCFE>2.0.CO;2.

Whiteman, D. N., 2003: Examination of the traditional Raman lidar technique. I. Evaluating the temperature-dependent lidar equations. *Appl. Opt.,* **42,** 2571–2592, doi:10.1364/AO.42.002571.

——, and Coauthors, 1992: Advanced Raman water vapor lidar. *16th Laser Radar Conf.,* Cambridge, MA, NASA Conf. Publ. 3158, 483–484.

——, and Coauthors, 2004: NASA/GSFC Scanning Raman Lidar measurements of water vapor and clouds during IHOP. *22nd Int. Laser Radar Conf.,* Matera, Italy, Optical Society of America, 337.

——, and Coauthors, 2006: Raman lidar measurements during the International H_2O Project. Part I: Instrumentation and analysis techniques. *J. Atmos. Oceanic Technol.,* **23,** 157–169, doi:10.1175/JTECH1838.1.

Zhang, D.-L., and W.-Z. Zheng, 2004: Diurnal cycles of surface winds and temperatures as simulated by five boundary layer parameterizations. *J. Appl. Meteor.,* **43,** 157–169, doi:10.1175/1520-0450(2004)043<0157:DCOSWA>2.0.CO;2.

——, S. Zhang, and S. J. Weaver, 2006: Low-level jets over the mid-Atlantic states: Warm-season climatology and a case study. *J. Appl. Meteor. Climatol.,* **45,** 194–209, doi:10.1175/JAM2313.1.